Controls of Organofacies and Redox Conditions on Organic Matter Quality in the Toarcian Black Shales of the Paris Basin

Andrea Schito[a,b,*], Sveva Corrado[c], Natalia A. Vergara Sassarini[c,d,e], Simonetta Cirilli[f], Amalia Spina[f], Pauline Michel[d], Andrea Ceriani[g], Enrique Gomez-Rivas[a,b], Marta Gasparrini[h]

[a] Universitat de Barcelona, Department of Mineralogy, Petrology and Applied Geology, Carrer Martí i Franquès, s/n, 08028, Barcelona, Spain

[b] Institut de Recerca Geomodels, Universitat de Barcelona (UB), Carrer Martí i Franquès, s/n, 08028, Barcelona, Spain

[c] Università degli Studi "Roma Tre", Dipartimento di Scienze, Roma, Italy

[d] IFP Energies nouvelles, 1-4 Av. de Bois Préau, 92852 Rueil-Malmaison, France

[e] INAF, Osservatorio Astronomico di Padova, Vicolo dell'Osservatorio 5, 35122, Padova, Italy

[f] Università degli Studi di Perugia, Dipartimento di Fisica e Geologia, Via Alessandro Pascoli, 06123, Perugia, Italy

[g] Khalifa University, Earth Sciences Department, Abu Dhabi, 127788, United Arab Emirates

[h] University of Milan, Earth Sciences Department, via Mangiagalli 34, 20133 Milan, Italy

* *Corresponding Author:* andrea.schito@ub.edu

Abstract

This study presents a new geochemical and petrographic data from investigation on 41 lower to middle Toarcian organic-rich shale to understand how redox conditions across the eastern half of the Paris Basin. Rock-Eval pyrolysis, control organofacies and organic matter quality in the Paris basin. Kerogen types range from type II to type III, with marked lateral and vertical variations from the eastern basin margin toward the depocenter. Four organofacies associations were distinguished, showing a progressive shift from AOM-dominated assemblages, interpreted as reflecting anoxic to suboxic conditions and efficient preservation of marine organic matter, to phytoclasts- and terrestrial palynomorphs-rich assemblages, consistent with dysoxic to oxic conditions and poorer organic matter preservation. Reconstructed original TOC and HI values reach approximately15 wt.% and 700 mg HC/g TOC, respectively, in the eastern sector, indicate a first phase where restricted circulation and oxygen-depleted bottom waters favoured organic-matter accumulation and preservation in the eastern sector while suboxic conditions promoted the preservation of AOM-rich organic matter but with llwer

TOC value in the depocenter. Later, dysoxic to oxic conditions reduced source-rock quality across the whole basin.
These results show that organofacies composition and redox-controlled preservation exerted a primary control on source-rock heterogeneity in the Toarcian black shales of the Paris Basin and can be used as an analogue for similar intracontinental basin.

Keywords: *Paris Basin, Toarcian black shales, organic petrography, organofacies, source rock quality, redox conditions*

1. Introduction

The Paris Basin (PB) is a reference for basin analysis studies of long-lasting, low subsiding basins developed in intracontinental settings (Mégnien,1980; Brunet and Le Pichon, 1982; Perrodon and Zabek, 1991; Guillocheau et al., 2000; Delmas et al., 2002, for a review).

Since the 1970s, research on the subsidence and sedimentary fill of the PB has been driven by hydrocarbon exploration and production interests, as this basin hosts multiple oil and gas targets (Gabalda et al., 2011), as well as numerous productive reservoirs for geothermal energy (Lopez et al., 2010, Réveillère et al., 2013; Drouiller et al., 2019; Wendebourg & Lamiraux, 2002). The main source rocks of the PB are hosted in the Mesozoic succession such as those of Hettangian/Sinemurian, Pliensbachian and Toarcian ages (Bessereau et al., 1995; Disnar et al., 1996). Among them, the best-known is the Lower Toarcian *Schistes Carton*. Early Toarcian deposition of organic-rich marine sediments has been widely recorded across Europe and is interpreted to be associated, at least in the first stages (Hermoso et al., 2013), with bottom water anoxic conditions related to environmental changes related to the so-called Toarcian Oceanic Anoxic Event (T-OAE). This event was first recognized by Jenkyns (1985; 1988) and is defined by means of the negative Carbon Isotope Excursion (CIE) observed at the base of the ammonite *serpentinum Zone* (Jenkyns, 1988). The *Schistes Carton* of the PB were deposited in one of the depocenters established during the early Toarcian in the area that is now mainly north-central Europe. These unit has historically been the focus of pioneering studies on the reactions kinetic driving the thermal evolution of organic matter (OM), as well as Rock-Eval, and molecular geochemical characterization (e.g. Tissot et al. 1971; Madec and Espitalié 1984; Hollander et al. 1991). The black shales deposition during the CIE was followed by at least three additional organic-rich depositional events during the early Toarcian arriving up to the *Bifrons* zone at the base of the Middle Toarcian (Hermoso et al. 2013).

Despite the large body of Rock-Eval and molecular geochemical data available for the Toarcian black-shales of the Paris Basin (e.g. Tissot et al. 1971; Madec and Espitalié 1984; Hollander et al.

1991; van Breugel et al. 2006; Hermoso et al. 2013; 2014), comparatively little is known about theabout their organofacies composition of the Toarcian black shales from the Paris Basin. An exception is the recent work of Fonseca et al. (2021), which studied the onset of the T-OAE interval in a well located in the easternmost part of the basin margin, where the Total Organic Content (TOC) often exceeds 10%.On the other hand, little is known about the environmental conditions during black shales deposition in other sectors across the whole basin and after the CIE excursion, and thus a knowledge gap remains on the relationship between source rock quality and environmental conditions (i.e., redox conditions, primary productivity, OM preservation) across different areas of the basin. This can be applied on similar intracontinental basins in the world.

To address this gap, we combine Rock-Eval pyrolysis, reflected-light organic petrography, transmitted-light palynofacies analysis and thermal-maturity correction of TOC and HI for Toarcian organic-rich shales from eight wells along a W–E transect across the Paris Basin. The aims are to: (i) characterize lateral and vertical changes in organic-matter composition; (ii) assess how organofacies relate to source-rock quality; and (iii) evaluate the role of depositional redox conditions and basin paleogeography in controlling organic-matter preservation.

2. Geological setting

The PB (Fig.1) is the largest onshore sedimentary basin in France (~110.000 km^2) that covers the northern half of the French territory. It is a nearly circular intracontinental basin that developed from Permian-Triassic to Middle Oligocene times through the deposition of marine, brackish, and continental sediments. This succession fills Carboniferous and Permian troughs and unconformably overlies the Paleozoic basement, interpreted as the northern branch of the Variscan orogen (Brunet & Le Pichon, 1982; Cazes et al., 1986; Perrodon and Zabek, 1991; Guillocheau et al., 2000; Baptiste et al., 2016). The PB is bounded by major tectonic structures, such as the Variscan thrust front to the North, and the Upper Rhine Graben to the East (Andre et al., 2010), and is surrounded by four eroded Variscan massifs: the Armorican Massif to the west, the Massif Central to the south, the Vosges to the east and the Ardennes to the northeast (Fig.1a).

During the Mesozoic and Cenozoic evolution the Paris Basin underwent a long-term thermal subsidence that was locally perturbed by intraplate deformation (Guillocheau et al., 2000), including phases of subsidence and limited uplift during the Early to Middle Jurassic and Late Cretaceous times, followed by a major uplift phase during the Cenozoic. Several unconformities record the major tectonic events that took place during the Jurassic-Cretaceous transition (Late Cimmerian phase), the Late Aptian (Austrian phase) and the Late Cretaceous to Early Tertiary (Laramide and Pyrenean phase) (Guillocheau et al., 2000, Fig. 1 b). These unconformities have been intepreted, as recording, respectively to (i) the early stage of the central North Atlantic rifting; (ii) a further stage of Atlantic Ocean opening and (iii) the Africa-Europe convergence (Perrodon and Zabek, 1991; Guillocheau et al., 2000).

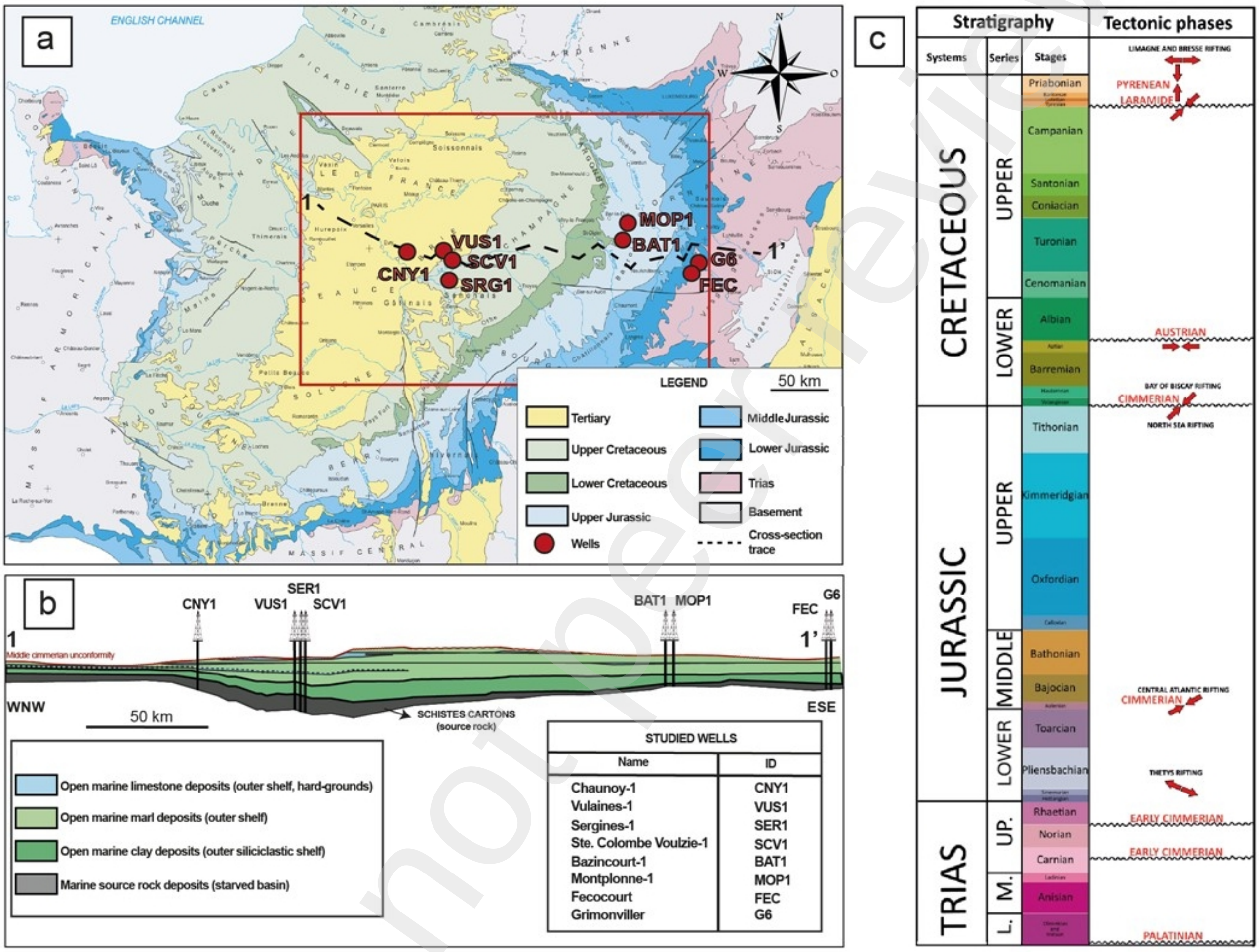

Figure 1a. Geological map of the Paris Basin (after BRGM, 1980) with location of studied wells (red dots), and traces of section 1-1' in b (dot-point black line); b. Geological cross-section of the Paris Basin (modified after Gely and Hanot, 2014 and Delmas et al., 2002) with projected studied wells. c. Main tectonic phases affecting the basin during the Mesozoic, modified after Delmas et al. (2002).

The latter phase was followed by Late Eocene-Early Oligocene E–W extension in the eastern part of the PB, related to the Rhine Graben opening (Sissingh, 2003), whereas a compressive regime was dominant to the west (Guillocheau et al., 2000; Andre et al., 2010). In detail, during the Eocene and part of the Neogene, in the so-called Laramide phase, Alpine and Pyrenean orogenic deformation resulted in positive inversion of several pre-existing structures, including the Bray and the Seine faults (Curnelle & Dubois, 1986; Fig. 1b, c).

The petroleum system of the PB depocenter hosts several main reservoir units: the Upper Triassic (Noran) fluvial sandstones of the Chaunoy Fm. (Bourquin et al., 1997; Vergara-Sassarini et al., 2024) and Donnemarie Fm., the deltaic to nearshore Rhaetiansandstones (Perrodon & Zabek, 1991; Novikoff et al., 2017), and the Middle Jurassic marine carbonates (Gaumet et al., 2001; Delmas et al., 2002; Mangenot et al., 2018; Beaudoin et al. 2019) whereas the principal hydrocarbon source rocks are the Lower Jurassic black shales, including the most widely studied Toarcian unit (e.g., *Schistes Carton*; Espitalié et al., 1988; Katz, 1995; Disnar et al., 1996).

Lower Toarcian organic-rich shales are widely distributed worldwide and record the onset of the T-OAE during the early *falciferum* Zone. This event is globally recognized by enhanced rates of organic carbon burial and a pronounced negative carbon-isotope excursion recorded in biogenic carbonates (Jenkyns, 1985; 1988, 2010; Jenkyns and Clayton 1986).

In the PB, the Lower Toarcian sediments are part of a first-order depositional cycle beginning in the Triassic and extending from the latest Carnian to the Toarcian, with a maximum of transgression in the early Toarcian time (Bessereau and Guillocheau, 1984). Lower Toarcian distal shales and marls deposited throughout the basin (Fig. 2), reach a maximum thickness of 70 m with TOC values mainly ranging from 3 to 7 wt% (Delmas et al., 2002; Bruneau et al., 2017). In such a contect, anoxia was probably controlled by low water circulation within the rapidly subsiding depocenters in deep sub-basins also associated with moderate primary productivity (Bruneau et al., 2017, 2018).

2.1 Wells' stratigraphy

Eight wells were selected along a W-E transect (Fig. 1 a), going from the main basin depocenter (to the E of Paris) to the eastern margin (in the Lorraine region), and for which cuttings of Lower to Middle Toarcian age are available from the *Geochim* database of *IFP Energies nouvelles*. From the westernmost to the easternmost the wells along the transect are: Chaunoy1 (48º34'0.5''N 2º48'12''E; CNY-1), Vulaines1 (47º38'40''N 3º51'44''E; VUS-1), Ste Colombe Voulzie (47º27'35''N 3º54'00''E; SCV-1), Sergines (48º05'38''N 4º54'49''E; SER-1), in the depocentral zone, Bazincourt (47º36'18''N 5º45'40''E; BAT-1) and Montplonne1(47º38'54''N 5º45'44''E; MOP-1) in the central zone (from now onward names as middle zone) and Grimonviller (47º18'31''N 6º36'57''E; G6) and Fecocourt (48° 24′ 13″ N 6° 01′ 15″ E; FEC) in the eastern margin. In FEC well we don't have the exact dept but samples come from the very first centimetres and depths can be approximated to zero (see Table 1).

Stratigraphy of the studied wells derived from IFP owned drilling reports and from the public French database of subsurface data (https://infoterre.brgm.fr/; Fig. 2), with the exception of the SER-1 well, for which stratigraphic information is unavailable.
The three wells drilled from the depocenter (CNY-1, VUS-1, SCV-1), show the most continuous stratigraphy from the Triassic up to the Cenozoic.

Where present, Triassic sediments are represented by intercalated siltstones and mudstones or by dolostones and anhydrites from the Keuper-Muschelkalk-Bunsandstein north European evaporitic series. They are generally overlaid by Lower Jurassic shales ending with Toarcian black shales (Fig. 2). Lower Toarcian black shales (i.e., *Schists Cartons)* occur in all the wells and, namely, are the only lithologies present in the easternmost and shallowest FEC and G6 wells (Fig. 2). The boundary with the Aalenian is marked by the Mid-Cimmerian unconformity. In the depocenter, the unconformity is characterized by the presence of hardgrounds in well CNY-1, is a paraconformity in VUS-1, while it marks an angular unconformity between the Middle Toarcian and the Aalenian-Bajocian in the SCV-1 well and in the middle sector. Upper to Middle Jurassic is composed almost exclusively of limestones in MOP-1 and BAT-1 wells (Fig. 2), while time-equivalent intercalations of siltstones and marls are present in CNY-1 and SCV-1 wells. At the top, the Neo-Cimmerian unconformity separates the lowermost Cretaceous succession from mostly Tithonian rocks, and this boundary represents the top of the two wells in the middle sector. The Lower Cretaceous succession is composed of 200 m of limestone in the CNY-1, while in the VUS-1 and SCV-1 wells the so-called Austrian unconformity separates Cenomanian to Albian shaly limestones and sandstones from Aptian to Neocomian shales, sandstones, and marls. The thickness of the Upper Cretaceous chalk below the Laramide unconformity (i.e., Alpine cycle) varies between 350 m in CNY-1 well and about 580-680 m in VUL-1 and SCV-1. Finally, the maximum thickness of Cenozoic is composed of 200 m of sandstones drilled in the CNY-1 well, while in SCV-1 and VUL-1 wells, it is about 80-60 m of Cenozoic limestone (Fig. 2).

3. Samples and methods

3.1 Investigated samples

41 cutting samples of the Lower to Middle Toarcian organic-rich shales and mudstones were collected from the eight studied wells (Figs. 1 and 2, Tab. 1). All selected samples have TOC values higher than 0.8 wt%; this information was retrieved from unpublished Rock-Eval 2 analyses from the *Geochim* database of *IFP Energies nouvelles*. Cavings and drilling contaminants effects were

minimized by kerogen concentration that physically separate drilling contaminants and statistical analyses for reflectance data (see Schito et al., submitted).

In this database, *Schistes Carton* are defined as those black shales deposited during the CIE (Tab. 1). The main limitation is that they are not defined by a specific biozone or by isotopic excursion, but simply by lithology and/or TOC values. Additionally, black shales deposited after the anoxic event were also sampled and may correspond to the main phases of organic-shales deposition that ended at the base of the Middle Toarcian, described by Hermoso et al. (2013) from the Couy-Sancerre well core located in the southern part of the basin.

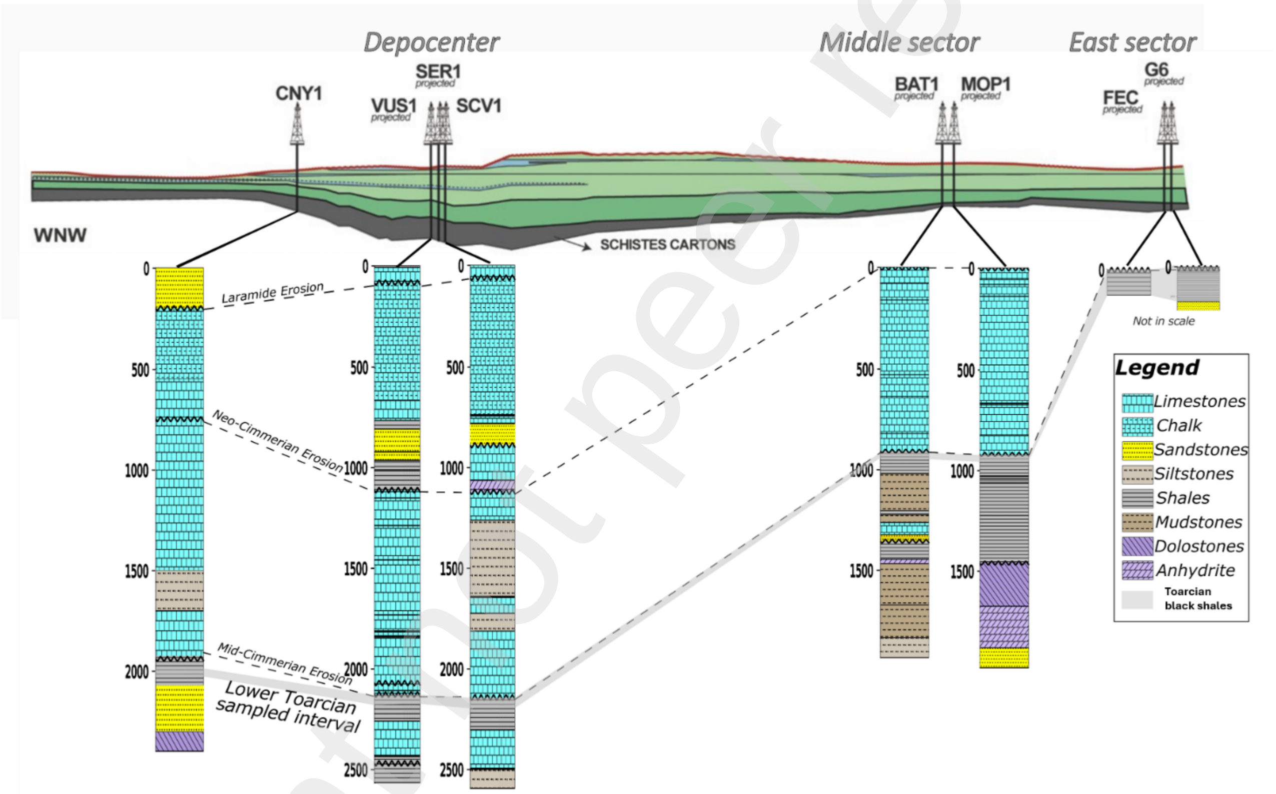

Figure 2 Well stratigraphy across the studied W-E transect of the PB with correlations of the main uncoformities (modified after Gely and Hanot, 2014 and Delmas et al., 2002), The grey area represents Lower to Middle Toarcian sampled stratigraphy. Numbers refer to depths in meters. FEC and G6 stratigraphies are not in scale.

3.2 Methods

3.2.1 Rock-Eval Pyrolysis

Each sample, constituted by about 60 mg of finely crushed bulk rock powder, was analyzed by means of the Rock-Eval 6 device (Lafargue *et al*., 1998; Behar *et al*., 2001; Romero-Sarmiento *et al*., 2016) to determine TOC (wt. %), HI (mg HC/g TOC), OI (mg CO2/g TOC) and T_{max} (ºC) from the S1, S2 and S3 (mg HC/g Rocks) peaks (Crumiere and Espitalié, 1989; Behar et al., 2001).

3.2.2 Organic petrography under reflected and transmitted light microscopy

Kerogen was concentrated from OM-rich shales for petrographic analyses under reflected and transmitted light.

For acid digestion, samples were washed, dried, slightly crushed and then concentrated through treatment with HCl (37%) and HF (50%) to extract kerogen (Traverse, 2007, Riding, 2021). The resulting kerogen was mixed, allowing the selection of a random portion of each specimen for a further room-temperature drying process, mounted on plexiglass plugs, embedded in a bi-component epoxy resin, and polished using three sandpapers and three alumina powders (1 μm; 0.3 μm, 0.1 μm grain sizes) for polishing.

Petrographic observation under reflected lights were performed on randomly oriented grains containing neither fractured nor oxidized macerals, using a Zeiss Axioplan microscope, under oil immersion (ν=1.518) in reflected monochromatic non-polarized light (λ = 546 nm), equipped with a J&M Analytik Tidas S 800 spectrometer CCD UV/NIR 2098 reflectance system. For reflectance analyses, three reflectance standards (Spinel %R_o= 0.426; Sapphire %R_o = 0.595; Yttrium-Aluminium Garnet %R_o= 0.905) were used for instrument calibration every 2hr. Random vitrinite reflectance and related standard deviation were derived from the arithmetic mean of measurements on indigenous fragments of telinite, collotelinite and collinite macerals. Furthermore, monochromatic light analysis has been integrated, when necessary, with fluorescent light analysis using the equipment Kübler codex_HXP 120.

Vitrinite-reflectance data for part of the dataset were previously reported by Vergara-Sassarini et al. (2023) and histograms' description of the in-situ vitrinite is provided in Schito et al. (submitted).

For transmitted light microscopic observations organic particles were classified according to their origin, using established palynofacies classification schemes (e.g., Whitaker, 1984; Steffen and Gorin, 1993; Tyson, 1995; Batten and Stead, 2005; Mendonça Filho et al., 2011; 2012). Relative abundances of the different organic constituents were determined by counting 300 particles per slide on two slides per sample. Samples were observed under a Nikon Labophot equipped with a blue-violet light with a wavelength of 395-440nm for fluorescence microscopy.

3.2.3 Original HI and TOC

Original HI values (HI_o) were estimated by using a kinetic correction model that accounts for thermal maturation by using the Transformation Ratio (TR; Jarvie; 2012; see below eq. 1). TR refers to the extent of conversion of kerogen into hydrocarbon and quantifies, in a dimensionless parameter, the progress of kerogen conversion into oil or gas depending on its thermal maturity. This parameter was calculated with the BasinMod 2D software by considering thermal calibration and the resulting burial history published in Schito et al. (submitted). To track petroleum generation through time, BasinMod 2D computes the forward-modeled TR dynamically by simulating the chemical cracking of organic matter as a function of the reconstructed thermal history. Through kinetics the cumulative conversion of kerogen is then continuously solved by the software, yielding the transient TR outputs as the fraction of generated hydrocarbons relative to the total generative potential of the source rock.

The relationship between measured and original HI is:

$$HI_o = \frac{HI_{measured}}{1 - TR} \qquad \text{eq. 1}$$

Similarly, original TOC values (TOC_o) are calculated through the TR by the formula:

$$TOC_0 = \frac{TOC_{measured}}{1 - TR} \qquad \text{eq. 2}$$

For the SER-1 well, where the lack of detailed stratigraphy hampered thermal modelling, TR was approximated to the Production Index (PI) that can be calculated as:

$$PI = {S_1}/{S_1 + S_2} \qquad \text{eq. 3}$$

4. Results

4.1 Rock-Eval Pyrolysis

Rock-Eval Pyrolysis results are reported in Table 1 and plotted in the modified van Krevelen diagram (OI vs. HI), and in the T_{max} vs. HI and TOC vs. S2 diagrams (Figs. 3A-D).

Types II, III and II-III are the dominant kerogen types characterizing the studied interval with HI values comprised in a wide range between ~100 and ~700 mg HC/g TOC, OI between 20 and 50 mg CO_2/g TOC and TOC between ~1 and ~13 wt% (Tab. 1).

In detail, data can be grouped into four groups:

(1) Group 1. The first group of samples from G6 and FEC wells (east sector) and most samples from MOP-1 well (middle sector), mainly exceed HI values of 600 mg HI/g TOC, indicating a type II kerogen tending towards type I. OI is mainly comprised between 20 and 35mg CO_2/g TOC. Data are more dispersed for the G6 well, where HI spans from ~500 to ~700 mg HC/g TOC. Thermal maturity of this group of samples from T_{max} indicates the immature stage of HC generation (Fig. 3b), except for the youngest MOP-1 sample, which indicates the onset of the oil window. TOC values from this group are the highest in the entire dataset and typically range from ~4 to ~14 wt%.

(2) Group 2. The second group of samples shows typical features of type II kerogen with HI between 400 and 550 mg HC/g TOC and OI between 10 and 25 mg CO_2/g TOC and come from greater depths of the three wells from the depocenter (SER-1, SCV-1, VUS-1, CNY-1; Figs. 3a and C). T_{max} thermal maturity falls in the early and mid-mature stages of HC generation (Fig. 3b). TOC is comprised between 3 and 5 wt%, with the exception of samples from the VUS-1 well, where TOC is between 1.5 and 2.0 wt% (Fig. 3d).

(3) Group 3. The third group shows typical features of type III kerogen with HI between ~150 and ~200 mg HC/g TOC and OI between 30 and 50 mg/g TOC. Samples belonging to this group are the shallowest in VUS-1, CNY-1, and SER-1; those from the BAT-1 well and one sample at the top of the sampled interval from MOP-1. Thermal maturity falls in the early and mid-mature stages of HC generation. TOC values are generally comprised between 1.0 and 1.2 wt.% (Fig. 3d).

(4) Group 4. The fourth group is characterized by intermediate features between type II and III kerogens with HI and OI values falling between those of groups 2 and 3, recorded only in wells CNY-1 and VUS-1 (Fig. 3a and c). T_{max} Thermal maturity falls in the early and mid-mature stages of HC generation (Fig. 3b). TOC values are generally comprised between 1.3 and 2.2 wt.% (Fig. 3D).

Well	**Sample**	**Depth (m)**	***TOC* (wt. %)**	***S1*** (mg/g Rock)	***S2***	***T_{max}* (°C)**	***HI* (mg HC/gTOC)**	***OI* (mg CO_2/gTOC)**	***R_o* (%)**	***%R_o sd***	***Nr* i. fr .**
	*CNY-1-1	2000	*2*	0.25	6.35	*429*	318	24	*0.55*	*0.06*	*32*
	CNY-1-10	2033	*3.44*	0.68	15.05	*432*	438	14	*0.60*	*0.06*	*28*
	CNY-1-11	2040	*3.35*	0.73	15.04	*433*	449	15	-	-	-
	***CNY-1-12**	2046	*4.21*	1.18	21.47	*433*	510	13	*0.59*	*0.05*	*26*
	CNY-1-13	2053	*3.99*	1.08	20.7	*434*	519	13	-	-	-
CHAUNOY 1	***CNY-1-14**	2056	*5.28*	2.05	28.03	*433*	531	11	*0.59*	*0.04*	*67*
	CNY-1-18	2026	*2.23*	0.28	7.91	*434*	355	45	-	-	-
	CNY-1-19	2036	*3.06*	0.57	12.24	*431*	400	21	-	-	-
	CNY-1-2	2006	*1.68*	0.19	4.78	*430*	285	25	*0.63*	*0.07*	*40*
	CNY-1-20	2043	*3.52*	0.83	16.69	*433*	474	16	-	-	-
	CNY-1-21	2046	*3.79*	0.84	19.02	*432*	502	17	-	-	-
	CNY-1-3	2008	*1.26*	0.11	2.66	*431*	211	33	*0.62*	*0.07*	*40*
	CNY-1-4	2010	*1.25*	0.13	2.39	*431*	191	35	-	-	-

	CNY-1-5	2013	1.1	0.09	1.67	433	152	43	-	-	-
	CNY-1-6	2016	1.19	0.12	1.9	434	160	37	-	-	-
	*CNY-1-7	2020	1.19	0.08	1.89	434	159	34	-	-	-
	CNY-1-8A	2023	1.5	0.14	2.8	433	187	31	-	-	-
	*CNY-1-9	2026	2.11	0.29	6.7	431	318	22	-	-	-
SERGINES 1	*SER-1-1	1913.4	0.86	0.07	1.6	435	186	41	0.66	0.05	21
	*SER-1-2	1916	0.99	0.09	2.1	433	212	31	0.65	0.07	29
STE COLOMBE VOULZIE	*SCV-1-1	2210	1.16	0.14	1.79	438	154	39	0.63	0.06	48
	***SCV-1-2**	2254	3.61	1.33	16.56	437	459	12	0.58	0.05	41
	***SCV-1-3**	2270	6.11	3.06	30.33	437	496	10	0.64	0.07	43
	***SCV-1-4**	2285	6.04	3.2	30.47	435	504	9	0.62	0.07	35
VULAINES 1	VUS-1-1	2136	1.55	0.25	6.47	433	417	21	-	-	-
	*VUS-1-2	2138	1.87	0.41	8.18	430	437	23	0.58	0.05	18
	*VUS-1-3	2150	1.33	0.28	4.45	433	335	32	0.65	0.05	31
	*VUS-1-4	2154	1.31	0.24	4.22	432	322	32	0.62	0.07	29
BAZINCOURT 1	*BAT-1-1	930	1.04	0.03	1.13	431	109	46	0.62	0.05	23
	*BAT-1-2	950	1.04	0.03	1.3	432	125	47	0.61	0.06	27
MONTPLONNE 1	*MOP-1-1	948	1.14	0.07	1.59	432	139	45	0.54	0.07	31
	***MOP-1-2**	1018	7.21	0.63	43.25	420	600	25	0.64	0.07	21
	***MOP-1-3**	1026	6.52	0.64	41.35	419	634	23	0.62	0.07	45
FECOCOURT	***FEC-1**	0	9.39	1.7	62.61	417	667	24	0.49	0.07	11
	***FEC-2**	0	13.89	2.34	93.3	421	672	25	0.43	0.06	40
	FEC-3	0	9.19	0.44	53.56	415	583	34	0.48	0.07	30
GRIMONVILLER	***G6-1**	7.25	7.93	0.9	49.72	423	627	25	0.49	0.04	41
	***G6-2**	14.85	4.63	0.32	25.88	425	559	28	0.54	0,04	29
	***G6-3**	21.7	9.53	1.63	68.49	421	719	23	0.52	0.06	45

*Table 1. Results of Rock-Eval pyrolysis and organic petrography. For each well sample name and depth, main pyrolysis parameters (S1, S2, TOC, T_{max}, HI, OI) and %Ro with standard deviation and number of indigenous humite-vitrinite fragments (Nr.i.fr.) are listed. In italic data already published in Vergara-Sassarini et al., 2023. * refers to samples on which transmitted light petrography on the concentrated fraction has been carried out. In bold samples referred to as Schistes Carton (i.e. Lower Toarcian) in the Geochim database.*

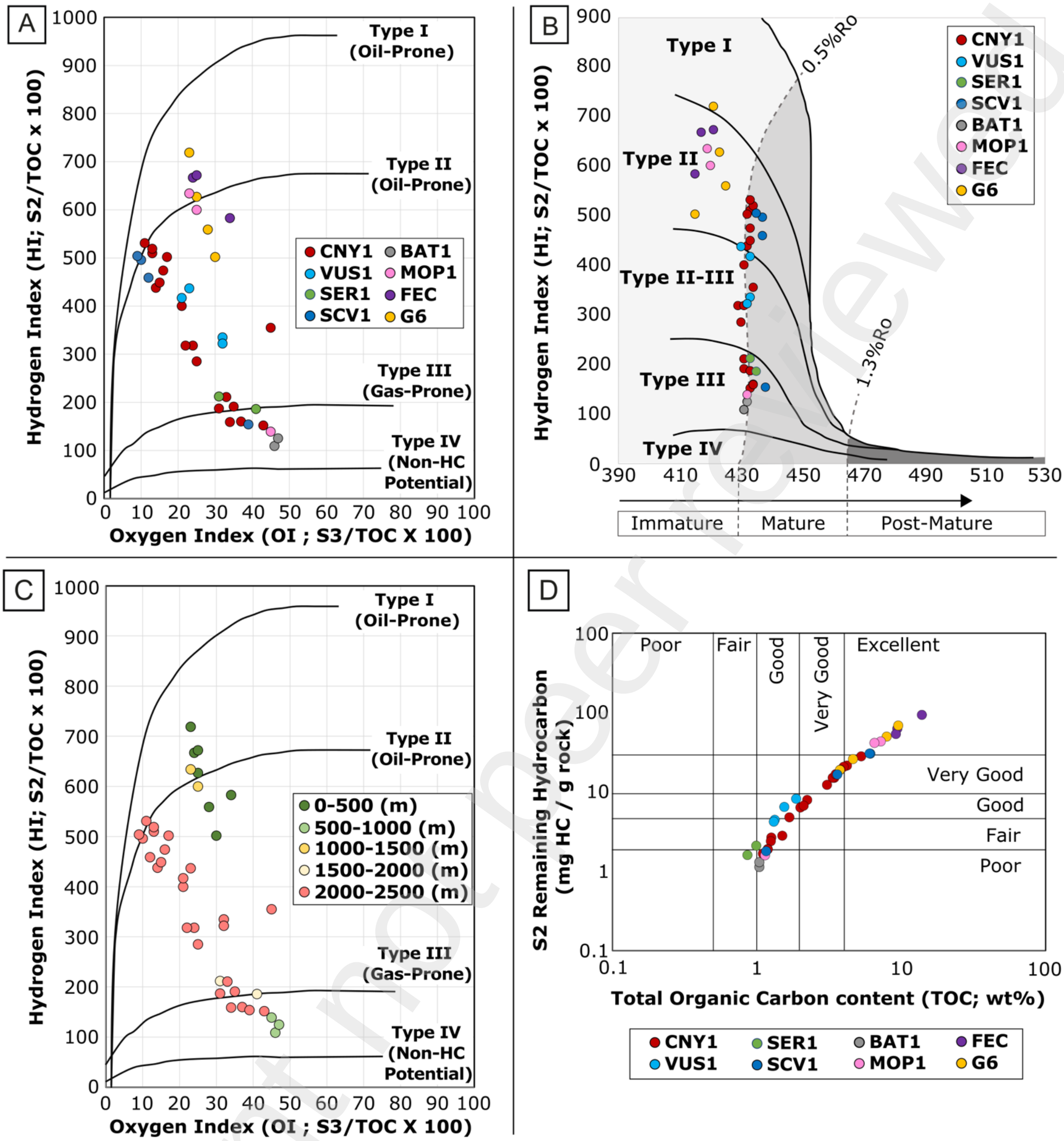

Figure 3 Cross-plots illustrating the relationships among the Rock-Eval pyrolysi parameters obtained from the 46 samples analyzed from eight wells. A) Modified van Krevelen diagram (OI vs HI) with samples colour-coded according to well location; B) T_{max} vs HI diagram, showing the thermal maturity distribution of the studied samples, grouped by ; C) Modified van Krevelen diagram (OI vs HI), with samples grouped into five depth classes; D) Petroleum potential diagram (TOC vs S2 peak) illustrating variations in source-rock quality and hydrocarbon-generating potential.

4.2 Reflected light analyses

Maceral description and %R_o results (Tab. 1, Figs. 4 and supplementary material) derive from a total of twenty-six selected samples (based on TOC and RE results) from the eight sampled wells and will be described according to the well location from E to W. %R_o data, are published in Vergara-Sassarini et al., (2023; Tab. 1). Here we integrate these data with description of maceral assemblages and reflectance variations. Mean reflectance, standard deviation, and number of measured fragments of the indigenous vitrinite are listed in Tab. 1, while their histograms are shown in (Schito et al., submitted).

4.2.1 Eastern basin margin (G6, FEC wells)

Petrographic investigation along the eastern basin margin focused on six samples from the G6 and FEC wells. The maceral composition in FEC and G6 wells is homogeneous and rich in AOM, characterized by a golden yellow color in fluorescent light and often associated with unoxidized pyrite framboids (Figs. 4 a and b). The liptinite group is present and shows high fluorescence, as in the prasinophytes *Tasmanite,* shown in Fig. 4c and d. Two families of vitrinite can be observed in both wells based on reflectance data: an indigenous one (dark grey) and a slightly lighter grey, reworked one (%R_o between 0.6 and 0.8%), which is more abundant than the first. Inertinite group fragments (e.g., mainly fusinite maceral) are present though not abundant (with %R_o always higher than 1.4%). The indigenous vitrinite family from FEC well samples shows a %R_o mean value ranging between 0.43 and 0.49 % and standard deviations between 0.06 and 0.07, while in the G6 well %R_o ranges between 0.46 and 0.54% with standard deviations between 0.04 and 0.06.

4.2.2 Middle sector of the transect (BAT-1, MOP-1 wells)

Samples from BAT-1 and the shallowest sample in MOP-1 show AOM with a weaker fluorescence than in the eastern sector (Fig. 4 e and f), and in the two deepest samples in MOP-1, where fluorescence is golden yellow and is often associated with not oxidized pyrite framboids.

The inertinite group is abundant as fusinite with %R_o generally between 1.0 and 2.0%, while vitrinite fragments belong to two populations, where the one with the lower %R_o has been interpreted as the indigenous one showing a mean value between 0.62 and 0.64% (Tab. 1) except in sample MOP-1-1 where the mean value is 0.55%. Standard deviation is between 0.05 and 0.07.

4.2.3 Depocentral zone (SER-1, SCV-1, VUS-1, CNY-1 wells)

In most of the samples from the depocentral sector, AOM is abundant and weakly fluorescing in most of the samples from the basin depocenter (Figs. 4 g to n). Highly fluorescing alginite (Fig. 4 h) or some sporinite also appear. Vitrinite is abundant, occurring as elongated fragments tens of microns in size (Figs. 4 I, j, k, l). %Ro values show a bi-modal distribution with the first, representing the indigenous fraction centered between 0.58 and 0.66 Ro (see Tab. 1) and the second, interpreted as the detrital fraction pointing to average values between 0.8 and 0.9%. The skewness of the indigenous fragment histograms points to standard deviations between 0.04 and

0.07 (Tab. 1). Fusinite and semi-fusinite macerals are also abundant but are smaller in size, and show %R_o values comprised between 1.1% and 1.8%.

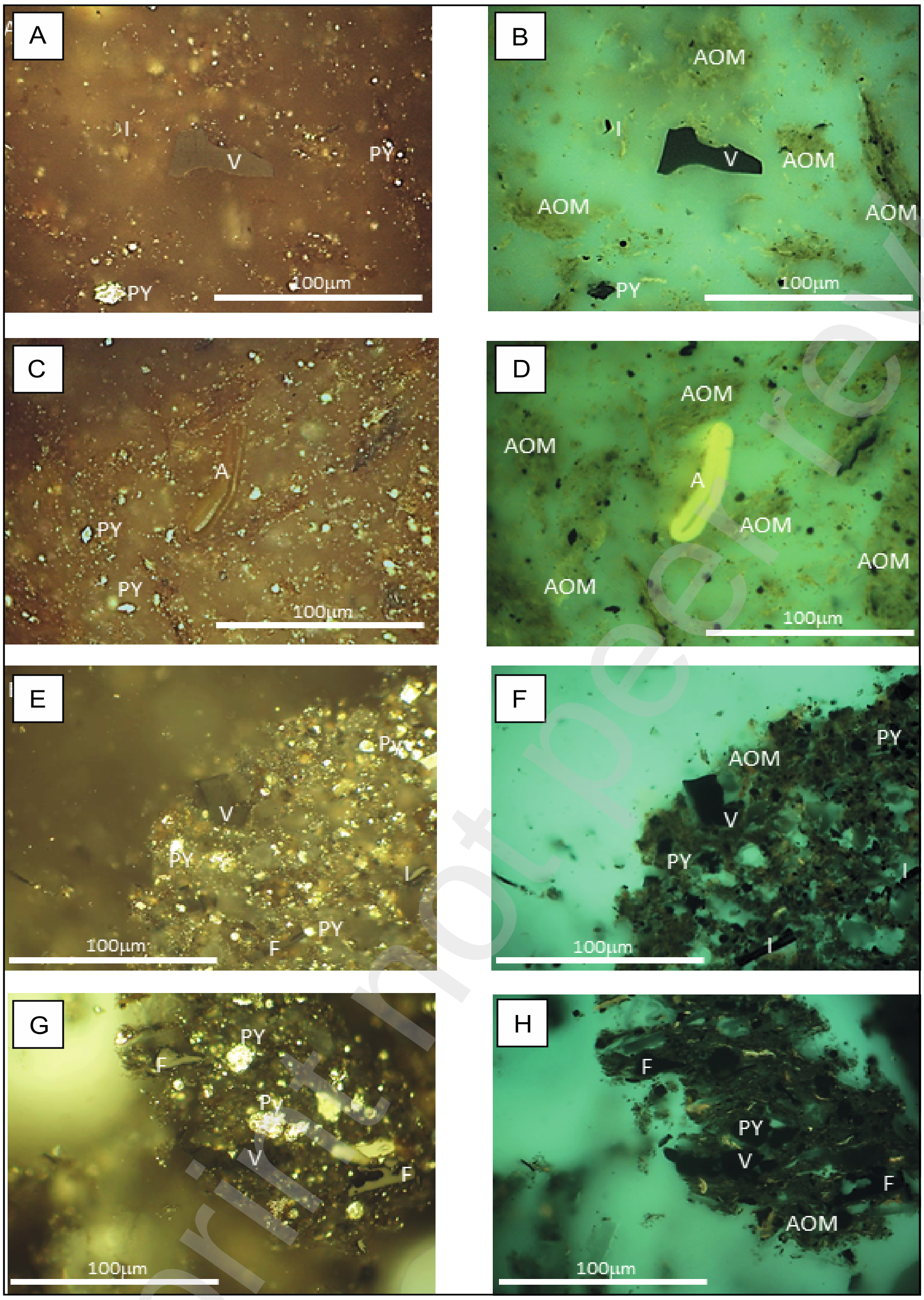

Figure 4 continues in the next page →

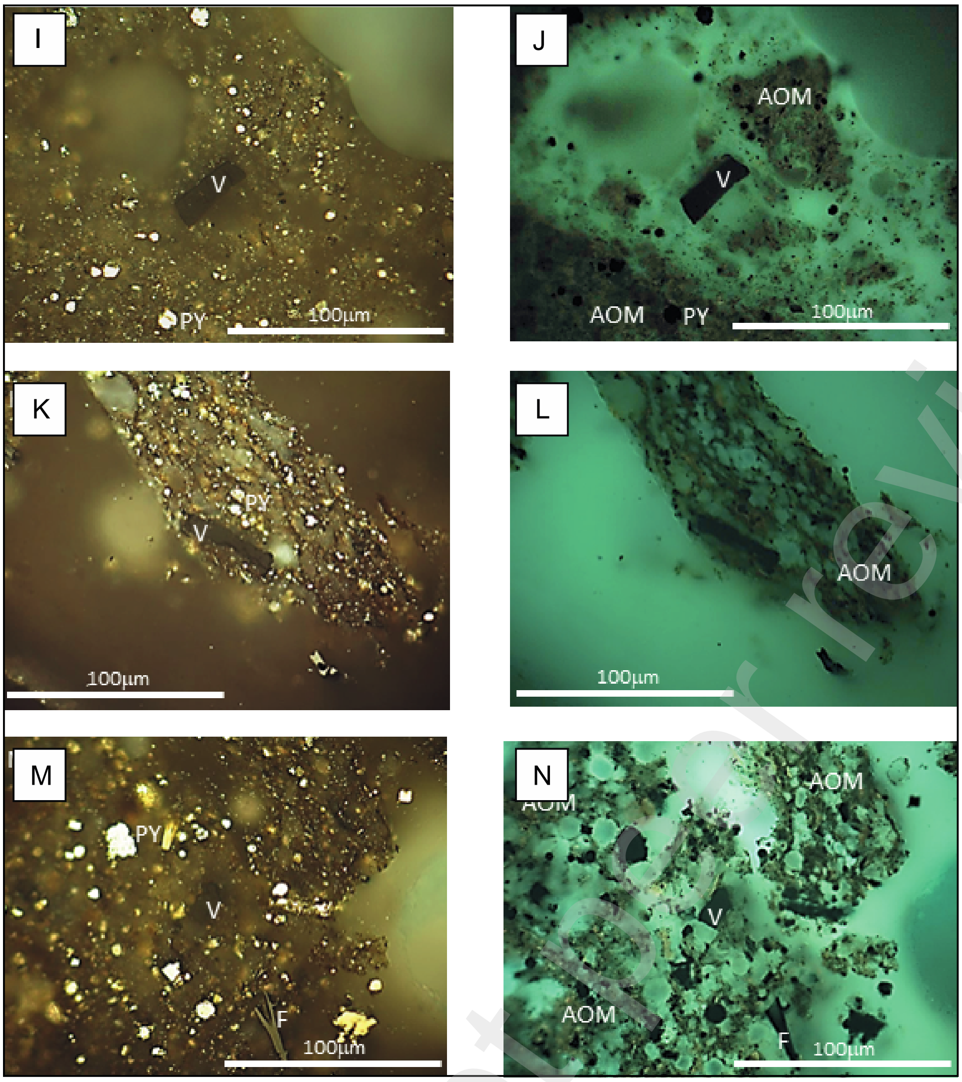

*Figure 4 Organic facies microphotographs representative of six of the studied Lower Toarcian samples, where V stands for huminite-vitrinite group fragment, I for inertinite group fragment, PY for pyrite, AOM for amorphous organic matter, A for alginite and F for fusinite. **A-B** (A- monochromatic and B-fluorescent light) FEC-1.2 sample. Note the AOM yellow fluorescent in B. **C-D** (C-monochromatic and D-fluorescent light) G6-3 sample. Note in the centre a bright yellow fluorescent alginite in amorphous organic matter matrix in D. **E-F** (E- monochromatic and F-fluorescent light) BAT-1.1 sample. Note the diffused golden yellow fluorescence of AOM in F. **G-H** (G- monochromatic and H-fluorescent light) SER-1.1 sample. **I-J** (I- monochromatic and J-fluorescent light) VUL-1.3 sample. **K-L** (K- monochromatic and L-fluorescent light) CNY-1.3 sample. **M-N** (M- monochromatic and N-fluorescent light) CNY-1_2 sample.*

4.3 Transmitted-light organic petrography

Semi-quantitative analyses of the organofacies in the eight analyzed wells were performed to cover all the sampled intervals (Tab. 1). Data are reported according to well location and are summarized in Table 2, where organofacies are divided into AOM, phytoclasts, and Palynomorphs. AOM has been further divided into two main categories according to its fluorescence properties. Phytoclasts have been classified into translucent and opaque, while palynomorphs have been classified depending on whether they derive from marine microplankton and zoomorphs or from terrestrial plants and freshwater microplankton. More details about the different organofacies can be found in the following text.

Table 2 Transmitted light semi-quantitative analyses. Acronyms: AOM amorphous organic matter; TP translucent phytoclasts; OP opaque phytoclasts; PAL terr terrestrial Palynomorphs; Pal mar, marine palynomorphs.

Well	***Sample***	**Organofacies (%)**						**Depth (m)**
		AOM		**Phytoclasts**		**Palynomorphs**		
		High Fluorescence	**Moderate Fluorescence**	**Translucent**	**Opaque**	**Terrestrial**	**Marine**	
CHAUNOY 1	CNY-1-1	0	47	17	32	4	1	2000
	CNY-1-7	9	28	17	16	17	13	2020
	CNY-1-9b	6	55	7	16	11	5	2026
	CNY-1-12	28	58	2	3	8	7	2046
	CNY-1-14	18	47	6	14	9	7	2056
VULAINES 1	VUS-2	24	59	3	5	2	8	2138
	VUS-3	17	46	5	7	5	18	2150
	VUS-4	9	58	7	14	7	2	2154
SERGINES 1	SER-1-1	2	54	8	20	11	3	1913
	SER-1-2	2	57	9	19	5	8	1916
STE COLOMBE VOULZIE	SCV-1-1	4	49	8	16	13	6	2210
	SCV-1-2	3	51	6	7	11	21	2254
	SCV-1-3	5	67	5	6	6	10	2270
	SCV-1-4	15	50	3	6	11	9	2285
BAZINCOURT 1	BAT-1-1	9	45	11	13	7	11	930
	BAT-1-2	6	36	8	15	13	15	950
MONTPLONNE 1	MOP-1-1	4	46	11	15	12	10	948
	MOP-1-2	82	4	3	7	2	>1	1018
	MOP-1-3	76	6	3	4	6	5	1026
FECOCOURT	FEC-3	93	0	1	2	1	2	>1
	FEC-1	93	0	2	3	>1	3	>1
GRIMONVILLER	G6-1	80	0	1	3	6	8	7.25
	G6-2	76	0	3	4	8	8	14.85
	G6-3	92	0	2	4	1	1	21.7

As a general description, from Table 2 a trend in organofacies composition has been depicted moving from the eastern margin to the depocenter showing a decrease in total AOM content at expense of total phytoclasts and palynomorphs. A similar trend is also observed in most of the wells in the depocenter and the middle zone moving from the bottom to the top. Moreover, the samples with the highest AOM content also show the highest percentage in fluorescing AOM.

4.3.1 Eastern basin margin (G6, FEC wells)

Samples from the eastern margin are characterized by a predominance of AOM over palynomorphs and phytoclasts. The organofacies associations are quite similar in all the samples: in the two samples from the FEC well and in G6-3, AOM represents more than 90% of the fragments and both phytoclasts and palynomorphs range between 1 and 4%. In samples G6-1 and G6-2, the AOM content drops to between 76% and 80%, with a slight increase in palynomorphs. AOM is heterogeneous in all the samples, appearing usually dark under transmitted white light (Figs. 5 a-c) and highly fluorescent under blue light (Figs. 5 b-d). The aspect is dense most of the time with a plate form showing, in some cases, angular outlines (Figs. 5 e-f-g). Their surface can appear cratered, sometimes giving a pseudo-cellular appearance, as in Figs. 5 b-e-g. Palynomorphs are mainly marine and dominated by prasinophytes, in sample G6-2 and G6-1, where they reach dimensions of more than 50 µm (Fig. 5 h). Phytoclasts are rare, and opaque phytoclasts are the most abundant.

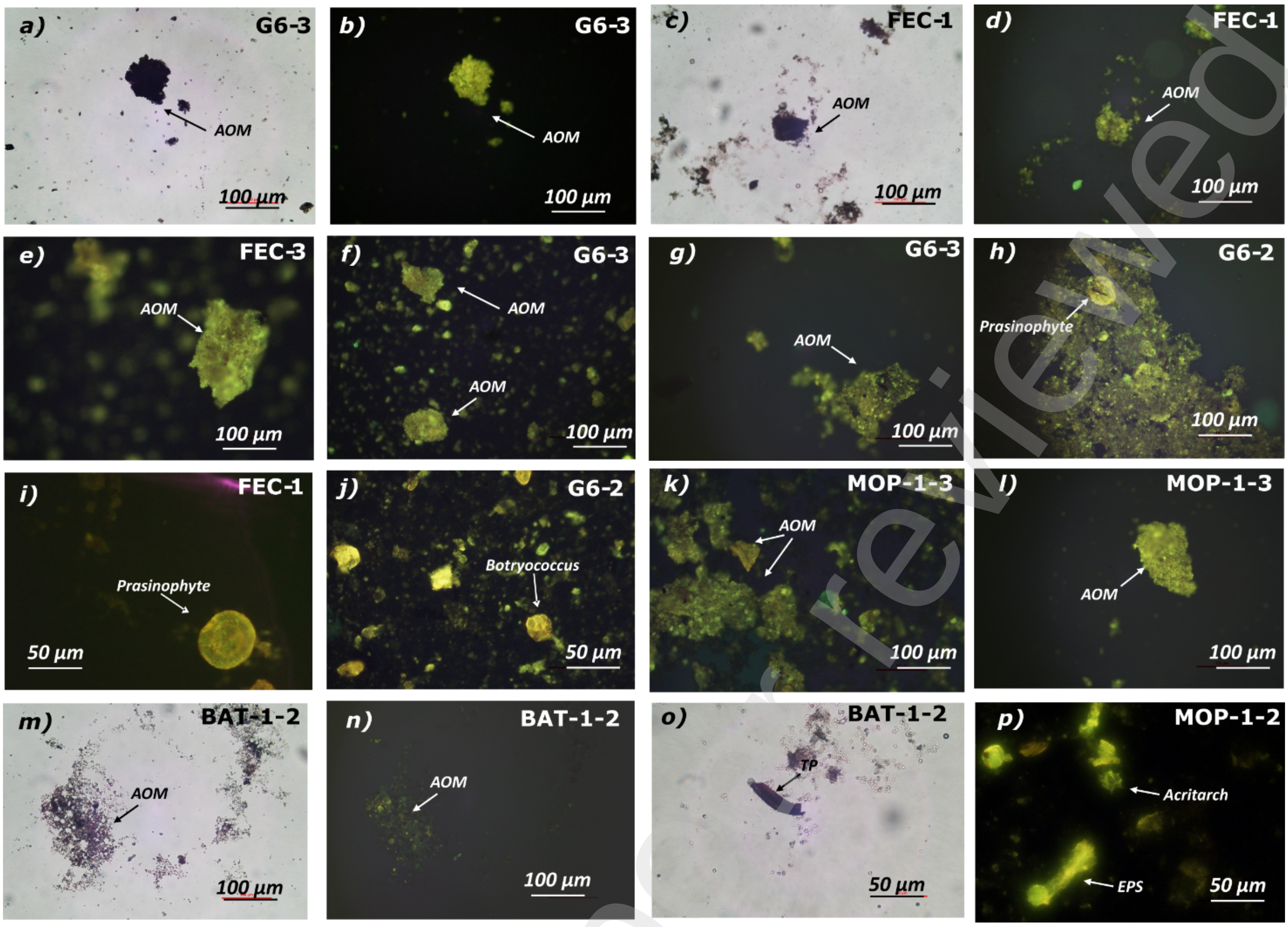

Figure 5 Transmitted-light and fluorescence data from the basin eastern margin and central sector. a) AOM in sample G6-3 under white light and b) showing intense fluorescence; c) AOM in sample FEC-1 under white light and d) showing intense fluorescence; e) fluorescing AOM in sample FEC-3; f-g) fluorescing AOM in sample G6-3; h) prasinophytes in a fluorescing AOM matrix in sample G6-2; i) prasinophytes in sample FEC-1; j) Botryococcus in sample G6-2 under fluorescence light; k-l) fluorescing AOM in sample MOP-1-3; m-n) non-fluorescing, granular, AOM in sample BAT-1-2; o) translucent phytoclasts in sample BAT-1-2; p) acritarch and EPS in sample BAT-1-2.

4.3.2 Middle sector of the transect (BAT1, MOP1 wells)

In the two wells of the middle sector a change in organofacies can be observed moving from the deepest samples in MOP-1 toward the shallower MOP-1-1 and the two samples in BAT-1 (Tab. 2). Samples MOP-1-2 and MOP-1-3 have a similar composition to the samples G6-1 and G6-2 of the eastern sector with a predominance of AOM, mostly fluorescing and with a plate shape as previously observed (Fig. 5 k-l). In the shallower samples, such fluorescing AOM becomes extremely rare, and a granular, non-fluorescing AOM with diffuse edges (Fig. 5 m-n) is the most abundant. Organofacies in these samples are characterized by a lower amount of total AOM and a total content of phytoclasts and palynomorphs always higher than 20% (Tab. 2). Translucent phytoclasts (Fig. 5 o) are common but always lower than opaque ones, and terrestrial palynomorphs such as spores appear together with the marine prasinophytes and acritarches (Fig. 5 p). Some structureless material with a diffuse outline and very high fluorescence has been interpreted as bacterial extracellular polymeric substance (EPS - Fig. 5 p) and has been counted together with the fluorescing AOM. To note this material is rare but have been found also in the samples of the eastern sector.

4.3.3 Main basin depocenter (SER-1, SCV-1, VUS-1, CNY-1 wells)

Samples from wells drilled in the depocenter have an organofacies content dominated by AOM which is higher than 50% in most of the samples except the two shallowest samples in CNY-1 (CNY-1-1, CNY-1-7; Tab. 2). Some fluorescing AOM, similar to that dominating in the eastern sector (Fig. 6 a-b), is still present even if in lower amounts, generally not exceeding the 10% apart the deeper samples in SCV-1 (SCV-1-4) and CNY-1 (CNY-1-12; CNY-1-14) and samples from VUS-1 (Tab. 2) where it reaches up to about 30%. However, the dominant AOM is granular, with weak fluorescence, diffuse edges, and palynomorph and phytoclast inclusions (Figs. 6 c-d). Granular AOM is sometimes observed in coexistence with fluorescing AOM (Figs. 6 e-f). Tentatively, a third kind of AOM can be recognized, characterized by a dark appearance under white light, more defined edges (Fig. 6 g), and very weak fluorescence (Fig. 6 h). Due to its scarcity, it has been counted among the weakly fluorescing AOM in Tab. 2.

Phytoclasts are generally small, with translucent phytoclasts (Figs. 6 i-j) slightly less abundant than the opaque ones that, in the shallowest samples of CNY-1 and SER-1, sometimes show preserved cell walls as in Fig. 6 k. In the same samples, some cuticles (Fig. 6 l) are rarely observed.

Prasinophytes (Fig. 6 m), followed by acritarchs (Fig. 6 n), are the most common among marine palynomorphs that dominated among the deepest samples in wells CNY-1, SCV-1 and VUS-1 (Tab. 2). On the other hand, terrestrial palynomorphs such as spores (Fig. 6 n-o) or pollen grains (Fig. 7 p) became more abundant toward the shallowest depths (Tab. 2).

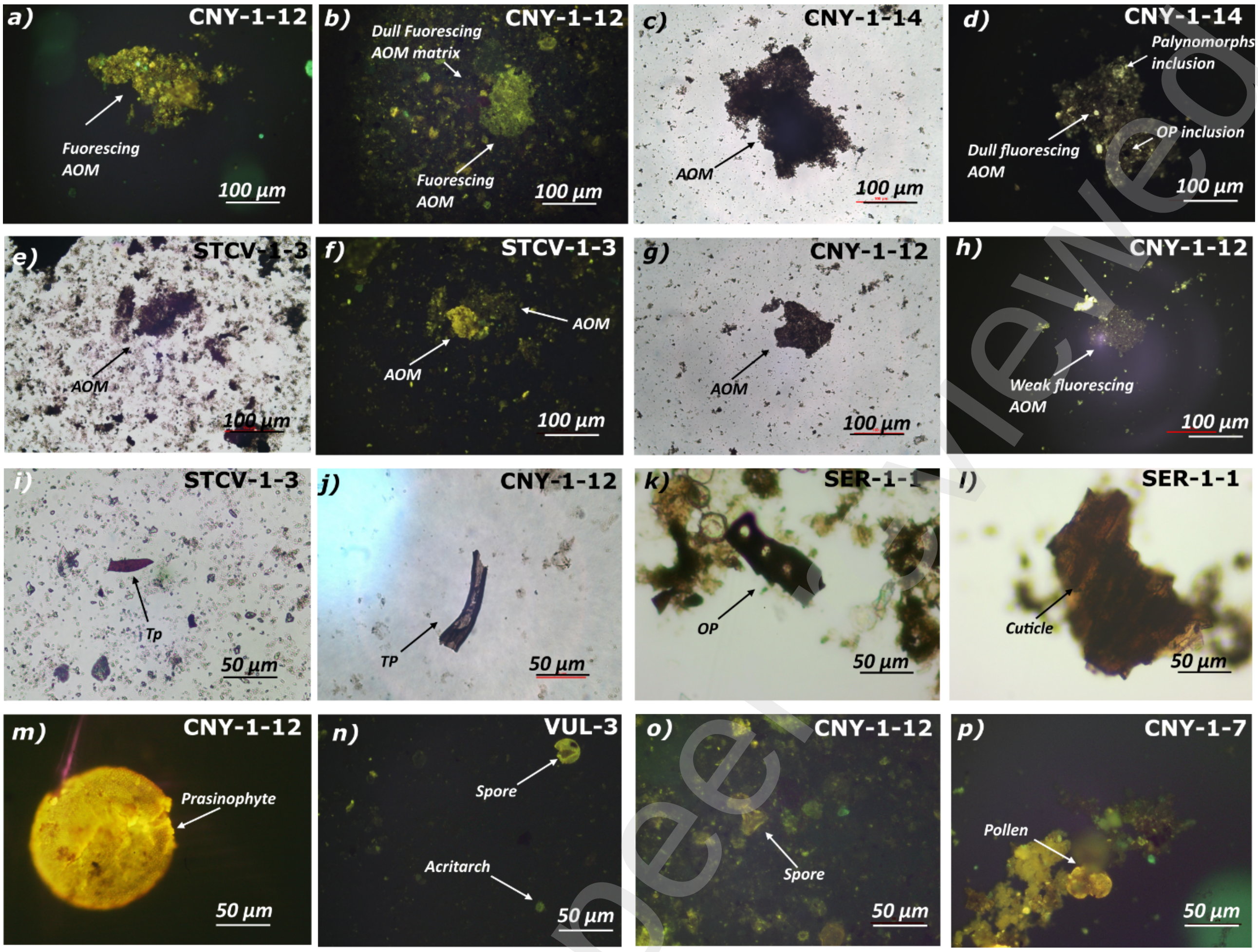

Figure 6 Transmitted-light and fluorescence data from the basin depocenter. a) Fluorescing AOM in sample CNY-1-12; b) fluorescent AOM within a weak fluorescing matrix in sample CNY-1-12; c) AOM in sample CNY-1-14 under white light and d) showing weak fluorescence and palynomorphs and phytoclasts inclusions under blue fluorescent light; e) AOM in sample SCV-1-3 under white light and f) showing both bright and weak fluorescence; g) AOM in sample CNY-1-12 under white light and f) showing weak fluorescence under blue light; i) Translucent phytoclasts in sample SCV-1-3 and j) CNY-1-12; k) opaque phytoclasts in sample SER-1-1;l) cuticle in sample SER-1-1; m) prasinophyte in sample CNY-1-12 under white light; n) acritarch and spore under fluorescent light in sample VUS-3; o) trilete spore in sample CNY-1-12 under fluorescent light; p) fluorescing pollen in sample CNY-1-7.

4.4 Original HI and TOC

The original HI and TOC (HI_o and TOC_o) were back-calculated after estimating TR from the burial history published in Schito et al. (submitted). The models were calibrated against the Toarcian vitrinite reflectance and T_{max} presented in this work (Fig. 3, Table 1), and point out that maximum temperatures were reached at the end of the Mesozoic, followed by an erosional phase during the Late Cretaceous to Oligocene (Schito et al., submitted) by using heat flow (HF) variation as in previous works (i.e. Torelli et al., 2020; Gonçalves et al., 2014). The calculated amount of erosion of the Mesozoic succession varies from the depocenter, where it accounts for a few hundred meters, to the eastern sector where it has been calculated of about 1.5 km. Eroded thicknesses, together with modeled heat flows (HF), TR values, HI_o and TOC_o are listed in Table 3.

Table 3 Calculated Transformation Ratio (TR) after thermal/burial modelling and Original HI (HI_o) and TOC (TOC_o) by using equations 1 and 2.

Well	**Sample**	**Depth**	***HF***	***Eroded thickness***	***TR***	***HI_o***	***TOC_o***
		(m)	***(mWm^3)***	***(m)***		***(mg HC/g TOC)***	***(wt%)***
CHAUNOY 1	CNY-1-1	2000	65	0	0.10	353	2.2
	CNY-1-10	2033			0.12	498	3.8
	CNY-1-12	2046			0.14	593	4.7
	CNY-1-14	2056			0.15	625	5.9
	CNY-1-2	2006			0.10	317	1.9
	CNY-1-3	2008			0.10	234	1.4
SERGINES 1	SER-1-1	1913.4			0.04	193	0.9
	SER-1-2	1916			0.04	220	1.0
STE COLOMBE VOULZIE	SCV-1-1	2210	65	0	0.20	193	1.2
	SCV-1-2	2254			0.22	588	4.0
	SCV-1-3	2270			0.24	653	6.8
	SCV-1-4	2285			0.24	668	6.7
VULAINE	VUS-1-2	2138	65	0	0.15	514	2.1
	VUS-1-3	2150			0.16	399	1.5
	VUS-1-4	2154			0.16	383	1.5
BAZINCOURT 1	BAT-1-1	930	70	1000	0.03	112	1.1
	BAT-1-2	950			0.03	129	1.1
MONTPLONNE 1	MOP-1-1	948	70	1000	0.05	146	1.2
	MOP-1-2	1018			0.05	632	8.0
	MOP-1-3	1026			0.06	674	7.3
FECOCOURT	FEC-1	0	75	1500	0.01	674	10.4
	FEC-2	0			0.01	679	15.5
	FEC-3	0			0.01	589	10.2
GRIMONVILLER	G6-1	7.25	75	1500	0.01	633	8.8
	G6-2	14.85			0.01	565	5.2
	G6-3	21.7			0.01	726	10.6

5. Discussion

5.1 Organic Matter Distribution and Organofacies Associations

Rock-Eval data (Tab. 1; Fig. 3) outline that the highest TOC and HI values occur in the eastern sector of the basin, particularly in the G6 and FEC wells and in the deepest samples of the MOP-1 well located in the middle sector. These levels are characterized by hydrogen-rich type II kerogen and exhibit very good to excellent oil-generating potential (Figs. 3a, b, d). Along the studied W-E transect, kerogen composition progressively changes from type II to mixed type II/III. Mixed kerogen is typical of the shallower samples from the middle sector (e.g., BAT-1 and MOP-1 wells) and of the deeper intervals within the depocentral wells (e.g., SCV-1, SER-1, VUS-1 and CNY-1 wells). The shallowest samples from both the depocenter (e.g., above 2025 m depth in CNY-1) and middle sector are dominated by gas-prone type III kerogen (Fig. 3c).

Similar lateral and vertical trends are observed in the reflected-light petrographic data. With only minor exceptions, samples from the eastern margin, together with the deepest intervals of the middle and depocentral sectors, show a predominance of AOM and fluorescing liptinite macerals (Tab.1 and Fig. 4). Conversely, shallower intervals in the BAT-1 and MOP-1 wells, as well as several samples from the depocentral area, display a greater contribution of terrestrial organic matter, as indicated by the increased abundance of vitrinite and inertinite macerals, particularly fusinite and semifusinite (Tab. 1).

To further constrain the organic matter composition and depositional conditions, semi-quantitative organic petrography under transmitted light was carried out. The results, integrated with TOC and HI data and plotted along the geological cross-section (Tab. 2; Fig. 7), reveal systematic changes in organofacies both laterally, from the eastern basin margin toward the depocenter, and vertically, from the lower to the upper parts of the succession in the intermediate and depocentral sectors.

Based on the relative abundance of AOM, phytoclasts and palynomorphs, four organofacies associations can be distinguished

Organofacies 1: Total AOM higher than 80%, predominance of strongly fluorescing AOM, phytoclasts and palynomorphs each generally less than 10%;

Organofacies 2: Total AOM higher than 60%, predominance of weakly fluorescing AOM, phytoclasts generally below 20%, marine palynomorphs typically more abundant than terrestrial forms;

Organofacies 3: Total AOM generally between 50 and 60%, predominance of weakly fluorescing AOM, phytoclasts higher than 20%, terrestrial palynomorphs generally more abundant than marine forms.;

Organofacies 4: Total AOM less than 50%, phytoclasts higher than 30%, dominance of terrestrial palynomorphs, only minor amounts of weakly fluorescing AOM. These organofacies associations define a clear trend from AOM-rich assemblages, indicative of enhanced preservation of marine organic matter, toward phytoclast- and terrestrial palynomorph-rich assemblages, reflecting increasing terrestrial input and progressively less favourable conditions for organic-matter preservation.

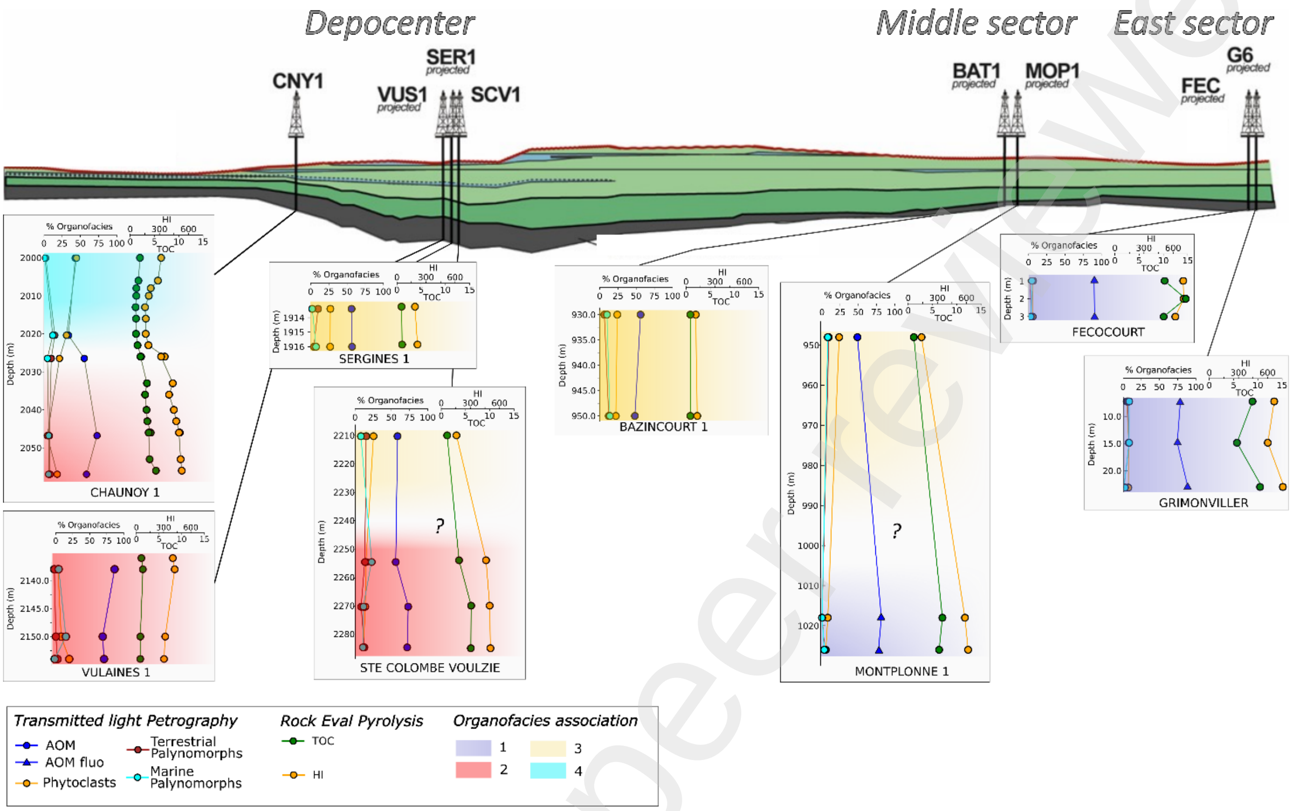

Figure 7 Organofacies and HI, TOC variation plotted for each well against depths. The coloured box indicate the organifaceis association dominating at different depths intervals. See the discussion for more details.

5.2 Geochemistry, Organic Matter Preservation and Source-Rock Quality

The organofacies associations defined above broadly correspond to the source-rock groups identified in section 4.1 by Rock-Eval Pyrolysis and provide important insights into the controls on organic-matter quality and preservation.

Organofacies 1 is primarily recorded in the eastern sector of the basin, where TOC values commonly exceed 10 wt.% and HI values are greater than 600 mg HC/gTOC (Fig. 7). Similar geochemical characteristics are also recorded in the deepest samples of the MOP-1 well in the intermediate sector, which are likewise assigned to Organofacies 1 (Fig. 7). These intervals represent the highest-quality source rocks recognized in the study area, as also indicated by the petroleum potential diagrams (Fig. 3). In contrast, the deepest samples from the depocentral wells (SCV-1, VUS-1 and CNY-1), assigned to organofacies 2, are characterized by lower TOC values (generally 2–6 wt.%) and HI values ranging between approximately 300 and 500 mg HC/g TOC. The decline in source-rock quality from the eastern margin toward the depocenter appears to reflect not only a decrease in the abundance of AOM but also changes in its composition and preservation state.

The highly fluorescent AOM observed in Organofacies 1 displays petrographic features including dense texture, dark appearance under transmitted light, plate-like morphology and locally cratered surfaces (Figs. 5 and 6). These characteristics resemble those described for bacterial-derived AOM by Mendonça-Filho et al. (2010, 2012). However, petrographic observations alone are insufficient to demonstrate a bacterial origin, and this interpretation should therefore be regarded as a working hypothesis pending confirmation by biomarker analyses. If a bacterial contribution was significant, the observed AOM may have formed through intense microbial productivity and subsequent heterotrophic reworking of extracellular polymeric substances (EPS) under oxygen-depleted conditions. Such processes are known to generate dense, strongly fluorescent AOM with high hydrocarbon-generating potential (Mendonça-Filho et al., 2010, 2012; Fonseca et al., 2018, 2020a, 2020b; de Andreade Lima et al., 2023). A similar organofacies was described by Fonseca et al. (2021) from Lower Toarcian deposits of the eastern Paris Basin, close to the area of MOP-1 and BAT-1 wells, and interpreted as recording enhanced microbial productivity during the initial stages of the T-OAE (the onset of the *Serpentinum* zone).
An alternative explanation is that the strongly fluorescent AOM reflects exceptionally efficient preservation of marine phytoplankton-derived organic matter under persistently anoxic conditions. In such a scenario, limited aerobic degradation would have preserved a large proportion of the original lipid-rich organic fraction, resulting in both high HI values and strong fluorescence. The available data do not allow discrimination between these two end-member models, and both mechanisms may have contributed to the observed organofacies.

Moving westward toward the depocenter, and upward within individual successions, the transition toward weakly fluorescent and more granular AOM is accompanied by increasing proportions of phytoclasts and palynomorphs. This trend may indicate either a reduction in microbial contributions, a greater contribution from phytoplankton-derived organic matter, or increasingly oxygenated conditions that promoted partial oxidation of labile organic compounds prior to burial.

Organofacies 3 occurs mainly in shallower intervals of the intermediate sector (above approximately 1000 m depth) and in the upper part of the depocentral wells (above approximately 2000 m depth; Fig. 7). These assemblages are characterized by lower abundances of AOM, higher proportions of terrestrial organic matter and correspondingly lower TOC and HI values, approaching the composition of mixed Type II–III and Type III kerogen. Organofacies 4 represents the most terrestrially influenced assemblages and is characterized by the lowest AOM contents and the poorest source-rock quality. These facies are best developed in the shallowest samples from the westernmost part of the study area, particularly in the CNY-1 well.

The relationship between organic petrography and source-rock quality is further illustrated in Figure 8, where samples are plotted on the Tyson (1995) ternary diagram. Most samples cluster toward the AOM apex, reflecting the predominance of marine organic matter and relatively reducing depositional conditions. The highest HI values occur within Organofacies 1, confirming that AOM-rich assemblages are associated with the greatest hydrocarbon-generating potential. According to Tyson (1995), such assemblages are commonly associated with suboxic to anoxic depositional environments characterized by enhanced preservation of marine organic matter.

Although AOM-rich facies are often associated with distal basinal settings, paleogeographic reconstructions of the Paris Basin during the Early Toarcian indicate that the eastern sector of the studied transect was relatively proximal t to emergent landmasses (Littke et al., 1991; Trabucho-Alexandre et al., 2012; Song et al., 2015). The scarcity of terrestrial particles in Organofacies 1 is therefore unlikely to reflect distance from sediment sources. Instead, it is more plausibly explained by dilution within exceptionally abundant marine-derived AOM, together with enhanced preservation under strongly reducing conditions.

The occurrence of *Botryococcus* and other freshwater-tolerant taxa (Fig. 5), together with previous geochemical studies (Hermoso et al., 2013; 2014; Fonseca et al., 2021), suggest periodic freshwater input and water-column stratification. Such conditions may have promoted nutrient accumulation, enhanced primary productivity and restricted bottom-water circulation, thereby favouring organic-matter preservation. These conditions appear to have extended from the eastern sector into at least part of the intermediate sector, including the MOP-1 area.

In contrast, Organofacies 2 from the depocentral wells records a greater abundance of marine palynomorphs, particularly prasinophytes and acritarchs, together with lower TOC and HI values (Fig. 8). These assemblages are consistent with suboxic conditions punctuated by episodic anoxia. The persistence of fluorescent AOM in the deepest depocentral samples suggests that reducing conditions were periodically established, although probably less persistently than in the eastern sector.

Finally, Organofacies 3 and 4 are interpreted to reflect a progressive deterioration in organic-matter preservation associated with increased oxygenation of bottom waters and greater terrestrial input. These facies may correspond to later phases of Lower Toarcian black-shale deposition that post-date the main T-OAE interval described by Hermoso et al. (2013). However, given the absence of robust biostratigraphic and chemostratigraphic constraints, this correlation should be regarded as tentative.

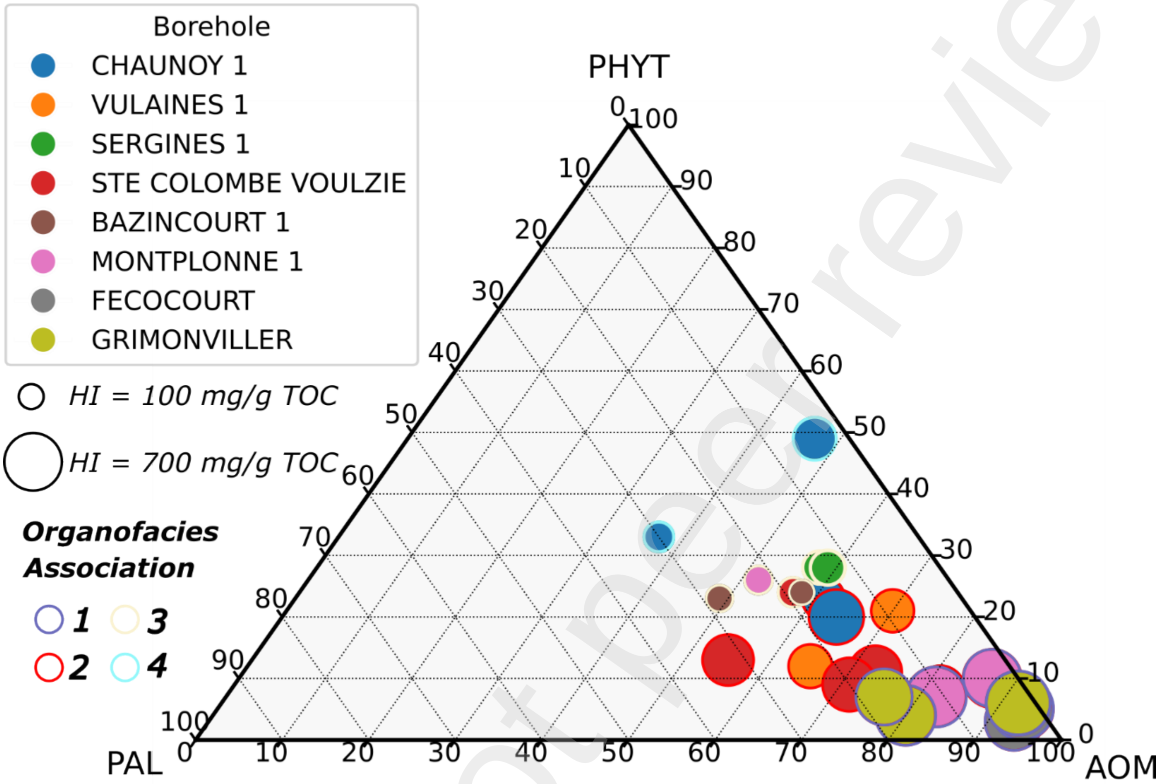

Figure 8 Ternary AOM-Phytoclasts-Palynomoprhs plot after Tyson (1995). Circles' diameters is a function of HI while the coloured rim links to the defined organofacies associations.

The lower HI values suggest more dysoxic/oxic conditions possibly related to the end of the transgression and the mix with more oxygenated water coming from the Neo-Thetys alternated to phases of low oxygen availability as suggested by the cyclicity of inorganic redox-sensitive proxies (i.e. Fe/Al; V/Al and Mo/TOC) in Hermoso et al. (2013). Finally, the increase of charcoals fragments (Fig. 6 k) in the opaque phytoclasts fraction in the shallow samples of the depocenter could be related with more arid climatic condition and increasing wildfire activity at the passage from the Early Toarcian to the early Middle Toarcian.

5.3 Depositional model and paleogeography

Thermal modelling constrained by the newly acquired Lower–Middle Toarcian (Torelli et al., 2020; Schito et al., submitted) maturity data indicates significant spatial variations in burial and thermal histories across the Paris Basin (i.e. HF and maximum burial, Fig. 9).

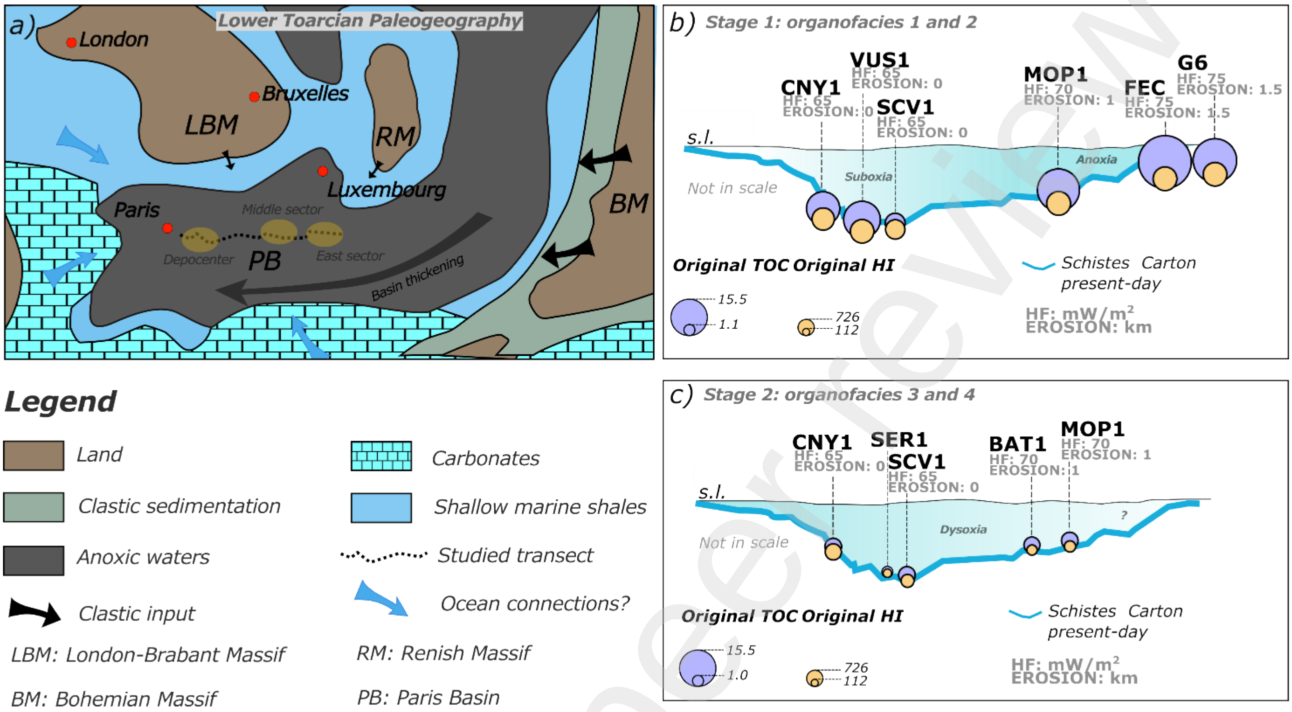

Figure 5 a) Lower Toarcian Paleogeography (redrawn after Song et al., 2017) showing the location of the three studied sectors with respect to emerged lands, clastic inputs and possible ocean connections; b) sketch (not to scale) summarizing the Original TOC and HI values and HF and eroded thicknesses in the basin after thermal modelling at the first stages of Toarcian black shales sedimentation. HF is measured in mW/m² and erosion in km ; c) sketch (not to scale) summarizing the Original TOC and HI values and HF and eroded thicknesses in the basin after thermal modelling at the second stages of Toarcian black shales sedimentation. HF is measured in mW/m² and erosion in km. Data in both figs. a and b are plotted against a schematic present-day stratigraphy (i.e. present-day depths of the Toarcian black shales).

The depocentral area experienced the greatest burial depths and the lowest amount of subsequent erosion, resulting in a longer residence time at maximum temperatures and, consequently, higher transformation ratios (TR). As a result, the differences between measured and reconstructed original TOC and HI values are expected to be the greatest in the depocentral wells.

The reconstructed original hydrogen index (HI_0) and total organic carbon (TOC_0) calculated using Eqs. 1–3 (Table 3), provide additional information on the depositional conditions that controlled organic-matter accumulation and preservation. Figure 9 b and c summarize the average HI_0 and TOC_0 values for each well and for the different stages of black-shale deposition identified through the organofacies classification.

It should be emphasized that the chronological framework of the studied intervals remains poorly constrained. The depositional stages discussed below are based primarily on stratigraphic position within the wells and on the classification of sampled intervals within the *Geochim* database. Consequently, direct correlation with the isotopically defined Toarcian Oceanic Anoxic Event (T-OAE) and the subsequent phases of black-shale deposition recognized by Hermoso et al. (2013) remains tentative and is beyond the scope of the present study.

Nevertheless, during the main phase of organic-rich shale deposition, the paleogeographic configuration of the Paris Basin was likely similar to that reconstructed by Song et al. (2017) based on previous studies (Littke et al., 1991; Trabucho-Alexandre et al., 2012). At that time, the Paris Basin formed the southern branch of the European epicontinental seaway, where widespread organic-rich sedimentation occurred. Accommodation space increased westward toward the depocenter, while the nearest emergent land areas were located north of the studied transect. To the south, carbonate platforms partially restricted exchange with the open Neo-Tethys Ocean (Fig. 9 a).

Assuming that the deepest samples from the depocentral and middle sectors are broadly coeval with those from the eastern sector, the organic petrographic and geochemical data suggest significant spatial heterogeneity in bottom-water conditions. The eastern and intermediate sectors are characterized by the highest reconstructed TOC_0 and HI_0 values and by Organofacies 1, indicating exceptionally efficient preservation of marine organic matter. These conditions may have resulted from enhanced primary productivity, stronger water-column stratification, prolonged bottom-water anoxia, or a combination of these factors. Following the model proposed by Fonseca et al. (2021), enhanced microbial productivity may have established a positive feedback mechanism in which elevated primary productivity increased oxygen consumption during degradation, thereby further intensifying anoxic conditions and promoting organic-matter preservation (Fig. 9 b).

In contrast, the depocentral sector is characterized by Organofacies 2, lower reconstructed TOC_0 values and HI_0 values generally ranging between 300 and 500 mg HC/g TOC. These assemblages contain abundant marine palynomorphs, particularly prasinophytes, which are commonly associated with stratified water columns and oxygen-depleted bottom waters. The coexistence of marine palynomorphs and weakly fluorescent AOM suggests suboxic conditions punctuated by episodic anoxic events rather than persistent water-column anoxia.

The observed differences in redox conditions may have been influenced by subtle paleobathymetric variations and by differences in water circulation across the basin. Although previous studies generally suggest limited bathymetric relief during the Early Toarcian, Fonseca et al. (2021) proposed that the eastern sector represented one of the most proximal areas of the basin. Under this scenario, restricted circulation and reduced water renewal may have favoured the development of more stagnant and oxygen-depleted conditions in the eastern and intermediate sectors. Conversely, the depocentral area may have experienced more effective water exchange, possibly through intermittent connections with the Neo-Tethyan realm. Such a mechanism could have periodically introduced relatively oxygenated waters into the basin, although the location and significance of these exchanges remain speculative (Fig. 9) and require further investigation.

The upper intervals of the studied successions record a progressive shift toward Organofacies 3 and 4, accompanied by lower TOC and HI values (Fig. 9 c). These changes indicate reduced preservation of marine organic matter, increasing terrestrial input and generally more oxygenated depositional conditions. In the westernmost part of the basin, represented by the CNY-1 well, the abundance of terrestrial organic particles suggests enhanced continental influence during this phase.

This transition likely reflects the progressive weakening of the environmental conditions that favoured organic-matter preservation during the main black-shale depositional interval. Previous studies have related this evolution to changes in basin circulation, reduced water-column stratification and increasing oxygenation of bottom waters during the later stages of the Early Toarcian (e.g., Guillocheau et al., 2000; Hermoso et al., 2013). Finally, the increased abundance of charcoal fragments observed in the uppermost samples may indicate enhanced wildfire activity and a shift toward more seasonally dry climatic conditions during the late Early Toarcian–early Middle Toarcian interval.

Conclusions

This study presents a new integrated geochemical and organic petrographic dataset from Lower Toarcian organic-rich shales of the Paris Basin, based on Rock-Eval 6 pyrolysis, reflected-light petrography and palynofacies analyses performed on samples collected from eight wells distributed along a regional west–east transect extending from the basin depocenter to its eastern margin.

The investigated interval displays significant lateral and vertical variations in organic-matter composition, source-rock quality and organofacies distribution. Kerogen types range from Type II to Type III, including mixed Type II–III assemblages. The highest source-rock quality occurs in the eastern and intermediate sectors of the basin, where TOC values reach up to 14 wt.% and HI values exceed 700 mg HC/g TOC. In contrast, lower TOC (generally 1–6 wt.%) and HI values characterize the depocentral and western sectors, where mixed Type II–III and Type III kerogen become progressively more abundant.

Thermal maturity data indicate that the studied succession is generally immature to early mature for hydrocarbon generation, with measured T_{max} values ranging from 415 to 438°C and vitrinite reflectance values between approximately 0.45 and 0.65% R_o.

Four organofacies associations were identified based on the relative abundance of amorphous organic matter (AOM), phytoclasts and palynomorphs. Organofacies 1, characterized by abundant strongly fluorescent AOM and the highest TOC and HI values, dominates the eastern sector and part of the intermediate sector. Organofacies 2 prevails in the depocentral area and contains abundant weakly fluorescent AOM together with marine palynomorphs, resulting in intermediate source-rock quality. Organofacies 3 and 4 are characterized by increasing terrestrial input, reduced AOM abundance and progressively lower hydrocarbon-generating potential.

The combined petrographic and geochemical data (including original HI and TOC) indicate that the spatial variability in source-rock quality was primarily controlled by differences in organic-matter preservation and depositional redox conditions. The eastern and middle sectors were likely characterized by strongly reducing conditions that favoured the accumulation and preservation of marine-derived organic matter, whereas the depocentral area experienced predominantly suboxic conditions punctuated by episodic anoxia. More oxygenated depositional conditions and increased terrestrial input characterized the later stages of black-shale deposition.

The origin of the highly fluorescent AOM remains uncertain. Petrographic characteristics are consistent with either a significant microbial contribution or exceptionally efficient preservation of marine organic matter under oxygen-depleted conditions. Additional biomarker studies are required to discriminate between these alternative interpretations.

Overall, the results demonstrate that the quality of Lower Toarcian source rocks in the Paris Basin was controlled not only by the quantity of preserved organic matter but also by variations in organofacies composition, redox conditions and basin-scale paleoenvironmental heterogeneity. These findings provide new insights into the mechanisms governing organic-matter enrichment within one of the most important Jurassic petroleum source-rock systems of Western Europe.

Acknowledgments

The research has also been funded by the public fundings of the Ramón y Cajal Program (RYC-2022) nº RYC2022-036094-I MINC/AEI/10.13039501100011033 and by the FSE+ given to the first author Andrea Schito, funded by the Spanish Ministry of Science and Innovation and cofounded by the European Union.

Part of the dataset was acquired during N.A. Vergara Sassarini PhD project, funded by: MUR grants to Roma Tre PhD School in Earth Sciences (XXXIV doctoral cycle, 2018–2021) and IFP Energies nouvelles PhD program.

IFP Energies nouvelles is acknowledged for fundings and for kindly providing access to samples, lab facilities and unpublished databases. Daniel Pillot and Herman Ravelojaona (IFP Energies nouvelles) are thanked for assistance during Rock-Eval sample preparation and analysis.

Andrea Schito thanks Platte River Associates for providing an academic licence of BasinMod 2D used to calculate original HI and TOC.

References

Andre, G., Hibsch, C., Fourcade, S., Cathelineau, M., Buschaert, S., 2010. Chronology of fracture sealing under a meteoric fluid environment: Microtectonic and isotopic evidence of major Cainozoic events in the eastern Paris Basin (France). Tectonophysics 490, 214–228.

Baptiste, J., Martelet, G., Faure, M., Beccaletto, L., Reninger, P.A., Perrin, J., Chen, Y., 2016. Mapping of a buried basement combining aeromagnetic, gravity and petrophysical data: The substratum of southwest Paris Basin, France. Tectonophysics 683, 333–348.

Batten, D.J., Stead, D.T., 2005. Palynofacies analysis and its stratigraphic application. In: Applied stratigraphy. Springer Netherlands, Dordrecht, pp. 203–226.

Beaudoin, N., Gasparrini, M., David, M.E., Lacombe, O., Koehn, D., 2019. Bedding-parallel stylolites as a tool to unravel maximum burial depth in sedimentary basins: application to Middle Jurassic carbonate reservoirs in the Paris basin. GSA Bull. 131, 1239–1254.

Behar, F., Beaumont, V.D.E.B., De B. Penteado, H.L., 2001. Rock-Eval 6 technology: performances and developments. Oil Gas Sci. Technol. 56, 111–134.

Bessereau, J., Guillocheau, F., 1984. Stratigraphie sismique et séquence de dépôt des séries liasiques du Bassin de Paris. Bull. Soc. Géol. Fr. 26, 607–616.

Bessereau, G., Guillocheau, F., Huc, A.-Y., 1995. Source rock occurrence in a sequence stratigraphic framework: the example of the Lias of the Paris Basin. In: Huc, A.-Y. (Ed.), Paleogeography, Paleoclimate, and Source Rocks. AAPG Studies in Geology, vol. 40. American Association of Petroleum Geologists, Tulsa, pp. 273–301.

Blaise, T., Izart, A., Michels, R., Suarez-Ruiz, I., Cathelineau, M., Landrein, P., 2011. Vertical and lateral changes in organic matter from the Mesozoic, eastern Paris Basin (France): variability of sources and burial history. Int. J. Coal Geol. 88, 163–178.

Bourquin, S., Vairon, J., Le Strat, P., 1997. Three-dimensional evolution of the Keuper of the Paris basin based on detailed isopach maps of the stratigraphic cycles: tectonic influences. Geol. Rundsch. 86, 670–685.

Bruneau, B., Chauveau, B., Baudin, F., Moretti, I., 2017. 3D stratigraphic forward numerical modelling approach for prediction of organic-rich deposits and their heterogeneities. Mar. Pet. Geol. 82, 1–20.

Bruneau, B., Villié, M., Ducros, M., Chauveau, B., Baudin, F., Moretti, I., 2018. 3D numerical modelling and sensitivity analysis of the processes controlling organic matter distribution and heterogeneity—A case study from the Toarcian of the Paris Basin. Geosciences 8, 405.

Brunet, M.F., Le Pichon, X., 1982. Subsidence of the Paris basin. J. Geophys. Res. Solid Earth 87, 8547–8560.

Cazes, M., Mascle, A., Torreilles, X., Bois, C., Damotte, X., Matte, P., Raoult, X., Pham, V.N., Hirn, A., Galdeano, X., 1986. Large Variscan overthrusts beneath the Paris basin. Nature 323, 144–147.

Crumiere, J.P., Espitalie, J., 1989. Characterization of organic depositional types based on the variation in the shape of the S2 peak of Rock-Eval pyrolysis. Results compared with data of optical surveys. C. R. Acad. Sci. Ser. II 309, 981–987.

Curnelle, R., Dubois, P., 1986. Évolution mésozoique des grands bassins sédimentaires Français; bassins de Paris, d'Aquitaine et du Sud-Est. Bull. Soc. Géol. Fr. 2, 529–546.

Delmas, J., Houel, P., Vially, R., 2002. Rapport regional d'évaluation pétrolière–Paris Basin Petroleum Potential. Institut Français du Pétrole Regional Report.

Disnar, J.R., Le Strat, P., Farjanel, G., Fikri, A., 1996. Organic matter sedimentation in the northeast of the Paris Basin: consequences on the deposition of the lower Toarcian Black Shales. Chem. Geol. 131, 15–35.

Drouiller, Y., Hanot, F., Gillot, E., Ferran, J.C., Michel, L., 2019. 3D seismic for design and derisking of dual geothermal boreholes in sedimentary sequences and new prospects in the Paris

Basin (Adapted methodology using petroleum industry techniques). Oil Gas Sci. Technol. 74, 32.

Espitalié, J., Maxwell, J.R., Chenet, Y., Marquis, F., 1988. Aspects of hydrocarbon migration in the Mesozoic in the Paris Basin as deduced from an organic geochemical survey. In: Organic Geochemistry In Petroleum Exploration. Pergamon, pp. 467–481.

Fonseca, C., Mendonça Filho, J.G., Lézin, C., Duarte, L.V., Fauré, P., 2018. Organic facies variability during the Toarcian Oceanic Anoxic Event record of the Grands Causses and Quercy basins (southern France). Int. J. Coal Geol. 190, 218–235.

Fonseca, C., Mendonça Filho, J.G., Lézin, C., Duarte, L.V., 2020a. Organic facies variability and paleoenvironmental changes on the Moroccan Atlantic coast across the Cenomanian—Turonian Oceanic Anoxic Event (OAE2). Int. J. Coal Geol. 230, 103587.

Fonseca, C., Mendonça Filho, J.G., Lézin, C., De Oliveira, A.D., Duarte, L.V., 2020b. Organic matter deposition and paleoenvironmental implications across the Cenomanian-Turonian boundary of the Subalpine Basin (SE France): Local and global controls. Int. J. Coal Geol. 218, 103364.

Fonseca, C., Mendonça Filho, J.G., Lézin, C., Baudin, F., de Oliveira, A.D., Souza, J.T., Duarte, L.V., 2021. Boosted microbial productivity during the Toarcian Oceanic Anoxic Event in the Paris Basin, France: new evidence from organic geochemistry and petrographic analysis. Geol. Soc. Lond. Spec. Publ. 514, 309–334.

Gabalda, S., Rigollet, C., Serrano, O., Audigane, P., Chiaberge, C., Courrioux, G., Truffert, C., 2011. Geological and petrophysical 3D modelling of sedimentary basins for groundwater applications, BRGM. In: 2011 GSA Annual meeting.

Gaumet, F., Garcia, J.P., Dromart, G., Allemand, P., 2001. Middle Jurassic production rates and «patchy» architecture of the carbonate systems along the north-western Tethyan margin (Paris basin to Sub-alpine basin). Géol. Méditerr. 28, 79–83.

Gély, J.-P., Hanot, F., 2014. Coupe Géologique du Bassin parisien et du Fossé hénan. In: Le Bassin parisien, un Nouveau Regard sur la Géologie, Paris, Association des Géologues du Bassin de Paris. Bull. Inf. Géol. Bass. Paris, Mémoire hors-série, v. 9, p. 1 plate.

Guillocheau, F., Robin, C., Allemand, P., Bourquin, S., Brault, N., Dromart, G., Grandjean, G., 2000. Meso-Cenozoic geodynamic evolution of the Paris Basin: 3D stratigraphic constraints. Geodin. Acta 13, 189–245.

Hermoso, M., Minoletti, F., Pellenard, P., 2013. Black shale deposition during Toarcian super-greenhouse driven by sea level. Clim. Past 9, 2703–2712.

Hermoso, M., Delsate, D., Baudin, F., Le Callonnec, L., Minoletti, F., Renard, M., Faber, A., 2014. Record of Early Toarcian carbon cycle perturbations in a nearshore environment: the Bascharage section (easternmost Paris Basin). Solid Earth 5, 793–804.

Hollander, D.J., Bessereau, G., Belin, S., Huc, A.Y., Houzay, J.P., 1991. Organic matter in the Early Toarcian shales, Paris Basin, France: a response to environmental changes. Rev. Inst. Fr. Pét. 46, 543–562.

Jarvie, D.M., 2012. Shale resource systems for oil and gas: Part 2—Shale-oil resource systems. In: Breyer, J.A. (Ed.), Shale energy resources: Processes, technologies, and research in the twenty-first century. AAPG Memoir 97, pp. 113–133.

Jenkyns, H.C., 1985. The Early Toarcian and Cenomanian-Turonian anoxic events in Europe: comparisons and contrasts. Geol. Rundsch. 74, 505–518.

Jenkyns, H.C., 1988. The early Toarcian (Jurassic) anoxic event; stratigraphic, sedimentary and geochemical evidence. Am. J. Sci. 288, 101–151.

Jenkyns, H.C., 2010. Geochemistry of oceanic anoxic events. Geochem. Geophys. Geosyst. 11, Q03004.

Jenkyns, H.C., Clayton, C.J., 1986. Black shales and carbon isotopes in pelagic sediments from the Tethyan Lower Jurassic. Sedimentology 33, 87–106.

Katz, B.J., 1995. The Schistes Carton—the Lower Toarcian of the Paris Basin. In: Petroleum Source Rocks. Springer Berlin Heidelberg, Berlin, Heidelberg, pp. 51–65.

Lafargue, E., Marquis, F., Pillot, D., 1998. Rock-Eval 6 applications in hydrocarbon exploration, production, and soil contamination studies. Rev. Inst. Fr. Pét. 53, 421–437.

de Andrade Lima, L.M.S., Vallejo, J.D., de Gusmão, R.B., Lima Filho, M.F., Piovesan, E.K., 2025. New palynological data and paleoenvironmental implications for the Lower Devonian and Lower Cretaceous successions in the Rio do Peixe Basin, Brazil: Sedimentary organic matter analyses. J. South Am. Earth Sci., 105805.

Littke, R., Leythaeuser, D., Rullkötter, J., Baker, D.R., 1991. Keys to the depositional history of the Posidonia Shale (Toarcian) in the Hils Syncline, northern Germany. Geol. Soc. Lond. Spec. Publ. 58, 311–333.

Lopez, S., Hamm, V., Le Brun, M., Schaper, L., Boissier, F., Cotiche, C., Giuglaris, E., 2010. 40 years of Dogger aquifer management in Ile-de-France, Paris Basin, France. Geothermics 39, 339–356.

Madec, M., Espitalie, J., 1984. Application of pyrolysis to the characterization and the upgrading of the Toarcian oil shales from the Paris basin. Fuel 63, 1720–1725.

Mangenot, X., Gasparrini, M., Gerdes, A., Bonifacie, M., Rouchon, V., 2018. An emerging thermochronometer for carbonate-bearing rocks:Δ 47/(U-Pb). Geology 46, 1067–1070.

Mégnien, C., Mégnien, F., 1980. Synthèse géologique du bassin de Paris: Lexique des noms de formation (Vol. 103). BRGM.

Mendonça-Filho, J.G., Chagas, R.B.A., Menezes, T.R., Mendonça, J.O., Da Silva, F.S., Sabadini-Santos, E., 2010. Organic facies of the Oligocene lacustrine system in the Cenozoic Taubaté basin, Southern Brazil. Int. J. Coal Geol. 84, 166–178.

Mendonça-Filho, J.G.M., Menezes, T.R., de Oliveira Mendonça, J., de Oliveira, A.D., da Silva, T.F., Rondon, N.F., da Silva, F.S., 2012. Organic facies: palynofacies and organic geochemistry approaches. In: Geochemistry–Earth's system processes. InTech, Rijeka, pp. 211–248.

Novikoff, T., Duboin, F.-A., Guion, C., Buisson, A., Dromart, G., 2017. Les environnements de dépôts margino-littoraux de la séquence du Rhétien du bassin de Paris The Marginal marine depositional environments of the Thaetic sequence in the Paris basin. Bull. Inf. Géol. Bass. Paris 54, 1–19.

Perrodon, A., Zabek, J., 1991. Paris Basin. In: Leighton, M.W., Kolata, D.R., Oltz, D.F., Eidel, J.J. (Eds.), Interior Cratonic Basins. AAPG Memoir 51, pp. 633–679.

Réveillère, A., Hamm, V., Lesueur, H., Cordier, E., Goblet, P., 2013. Geothermal contribution to the energy mix of a heating network when using Aquifer Thermal Energy Storage: modeling and application to the Paris basin. Geothermics 47, 69–79.

Riding, J.B., 2021. A guide to preparation protocols in palynology. Palynology 45, 1–110.

Romero-Sarmiento, M.F., Pillot, D., Letort, G., Lamoureux-Var, V., Beaumont, V., Huc, A.Y., Garcia, B., 2016. New Rock-Eval method for characterization of unconventional shale resource systems. Oil Gas Sci. Technol. 71, 37.

Sissingh, W., 2003. Tertiary paleogeographic and tectonostratigraphic evolution of the Rhenish Triple Junction. Palaeogeogr. Palaeoclimatol. Palaeoecol. 196, 229–263.

Schito, A., Corrado, S., Vergara Sassarini, N. A., Pauline, M., Cirilli, S., Spina, A., Ceriani, A., Gomez-Rivas, E., Gasparrini, M. Submitted. Thermal model dataset from a depocenter to eastern margin transect of the Paris Basin calibrated by Toarcian shales thermal maturity data. Data in Brief, Submitted.

Song, J., Littke, R., Weniger, P., Ostertag-Henning, C., Nelskamp, S., 2015. Shale oil potential and thermal maturity of the Lower Toarcian Posidonia Shale in NW Europe. Int. J. Coal Geol. 150, 127–153.

Song, J., Littke, R., Weniger, P., 2017. Organic geochemistry of the lower Toarcian Posidonia Shale in NW Europe. Org. Geochem. 106, 76–92.

Steffen, D., Gorin, G.E., 1993. Sedimentology of Organic Matter in Upper Tithonian-Berriasian Deep-Sea Carbonates of Southeast France: Evidence of Eustatic Control. In: Source Rocks in a Sequence Stratigraphic Framework. AAPG, Tulsa, OK, USA, pp. 49–65.

Tissot, B., Califet-Debyser, Y., Deroo, G., Oudin, J.L., 1971. Origin and evolution of hydrocarbons in early Toarcian shales, Paris Basin, France. AAPG Bull. 55, 2177–2193.

Torelli, M., Traby, R., Teles, V., Ducros, M., 2020. Thermal evolution of the intracratonic Paris Basin: Insights from 3D basin modelling. Mar. Pet. Geol. 119, 104500.

Trabucho-Alexandre, J., Dirkx, R., Veld, H., Klaver, G., de Boer, P.L., 2012. Toarcian black shales in the Dutch Central Graben: record of energetic, variable depositional conditions during an oceanic anoxic event. J. Sediment. Res. 82, 104–120.

Traverse, A., 2007. Differential sorting of palynomorphs into sediments: palynofacies, palynodebris, discordant palynomorphs. In: Paleopalynology. Springer Netherlands, Dordrecht, pp. 543–579.

Tyson, R.V., 1995. Sedimentary Organic Matter: Organic Facies and Palynofacies. Springer, Dordrecht.

van Breugel, Y., Schouten, S., Tsikos, H., Erba, E., Price, G.D., Sinninghe Damsté, J.S., 2006. Carbon isotope lithostratigraphy and characterization of organic matter across the early Toarcian oceanic anoxic event in the Paris Basin. Org. Geochem. 37, 1722–1739.

Vergara Sassarini, N.A, Schito, A., Gasparrini, M., Michel, P., Corrado, S., 2023. Automatic organofacies identification by means of Machine Learning on Raman spectra. Int. J. Coal Geol. 271, 104237.

Sassarini, N. A. V., Gasparrini, M., Bernasconi, S. M., & Corrado, S. (2024). Joint application of fluid inclusion and clumped isotope (Δ 47) thermometry unravels the complexity of thermal and fluid-flow history reconstruction in sedimentary basins—Upper Triassic Chaunoy Formation reservoirs (Paris Basin). *Basin Research*, *36*(1), e12814.

Wendebourg, J., Lamiraux, C., 2002. Estimating the ultimate recoverable reserves of the Paris Basin, France. Oil Gas Sci. Technol. 57, 621–629.

Whitaker, M.F., 1984. The usage of palynostratigraphy and palynofacies in definition of Troll Field geology. In: Reduction of uncertainties by innovative reservoir geomodeling. 6th Offshore Northern Seas Conference and Exhibition, Stavanger 1984. Norsk petroleumsforening, Paper G6, 44 pp.